A TALE OF TWO NUTRITIONAL TARGETS: STUDIES OF MOLECULAR STRUCTURE AND PEDAGOGY

by

SAYANTANI SARKAR

A dissertation submitted to the Graduate Faculty in Biochemistry in partial fulfillment of the requirements for the degree of Doctor of Philosophy,
The City University of New York

2012

This manuscript has been read and accepted for the
Graduate Faculty in Biochemistry in satisfaction of the
dissertation requirement for the degree of Doctor of Philosophy.

Dr. Ruth E. Stark

Date — Chair of Examining Committee

Dr. Edward J. Kennelly

Date — Executive Officer

Dr. Ranajeet Ghose, City College

Dr. Thomas Haines, City College

Dr. Judith Storch, Rutgers University

Dr. Yujia Xu, Hunter College

Supervisory Committee

THE CITY UNIVERSITY OF NEW YORK

Abstract

A Tale of Two Nutritional Targets: Studies of Molecular Structure and Pedagogy

by

Sayantani Sarkar

Advisor: Professor Ruth E. Stark

Nutrition is one of the allied branches of biochemistry. Numerous nutritional targets in lipid metabolism and energy homeostasis are widely studied in biochemical research. For instance, liver fatty acid-binding protein is an important player in lipid metabolism. In this dissertation, two nutritional targets: physiological liver fatty acid-binding protein (LFABP) and natural tomato were studied from basic research and pedagogical perspectives. Three different projects were undertaken involving LFABP and tomato. (1) In the first project, solution state NMR was used to investigate ligand binding to LFABP. Oleate and linoleate exhibited moderately different binding locations in spite of apparently similar binding stoichiometries to LFABP. Additionally, oleate liganded holo LFABP showed chemical shift perturbations in presence of the anticoagulant drug warfarin, indicative of possible competition between oleate and warfarin as ligands of LFABP. However, reported claims of glucose and phytanic acid as ligands of LFABP could not be validated by solution state NMR. (2) In the second project, the basic research protocol concerning LFABP inspired a redesign of the City College undergraduate biochemistry laboratory course with an aim to incorporate a "research-inspired" module involving a new in-silico exercise. (3) In the third project, basic physical and spectroscopic research techniques used to study biopolymers in tomato were used to develop an adaptable suite of chemistry

experiments for undergraduate and high school students. Both curricula were successfully tested on undergraduate and high school students in a cost effective fashion, demonstrating the feasibility of their implementation.

Dedication

I am dedicating this dissertation to the loving memory of my grandparents (Mr. Anil Kumar Das, Mrs. Durgesh Nandini Das, Mr. Bireswar Sarkar and Mrs. Santi Sudha Sarkar) and paternal uncle (Dr. Sundar Gopal Biswas).

Acknowledgements

First, I would like to extend my sincere gratitude to my mentor Distinguished Professor Ruth E. Stark for giving me this excellent opportunity to study protein ligand interaction by NMR. Apart from basic research, I am excited to get involved in Professor Stark's outreach activity by developing research-based curriculum to impart scientific knowledge to undergraduate and high school students. It gave me the opportunity to hone my pedagogical skills. I will always be grateful to Professor Stark for patiently guiding me with valuable insights and suggestions in each step of my graduate life.

I am thankful to my thesis committee members Profs. Dr. Ranajeet Ghose, Dr. Thomas Haines, Dr. Judith Storch, Dr. Yujia Xu for their advice throughout my graduate work. I would like to thank the Ghose group for sharing their equipment. I am thankful for being able to use the NMR facility at NYSBC. I would also like to thank Dr. Hsin Wang (NMR Facility Manager, CCNY) and Dr. Cedric Bérnard (Senior Research Associate, The Stark Group) for helping me learn minute details of experimental set-up, data processing and analysis. I am thankful to Dr. Bérnard for his insight and comments during the writing process. I am grateful to my colleagues at CCNY, the Stark group members- Samar, Silmilly, Moyouri, Sindy, Subhasish, Xudong, the Ghose group members and everybody else who helped me sail through this arduous path smoothly. I would also like to thank the staff members of Chemistry Department at CCNY and Biochemistry office at the Graduate Center for administrative support.

I am grateful to be able to find an elder sister in Dr. Mitali Chattopadhyay while far away from home. Mitali-di and her family with little Roosha, made my campus life joyous with all those home-cooked food and fun. Thank you so much Mitali-di for being there as a patient listener. I

would also like to thank my cousin Dr. Indranil Sarkar and his family for being there at my hours of need. I am grateful to Swarup-da for his support. I am indebted to Mr. Abhimanyu Basu & Mrs. Anamitra Basu for their graciousness.

I am grateful to numerous teachers; first, my grandma and grandpa- Mrs. Suroma Ghosh and Mr. Samar Ghosh. At College, Prof. Madhusudan Ghosal (MSG Sir), Prof. Tushar Kanti Ghosh (TKG Sir), Prof. Bhaswar Mukherjee, Prof. Mira Ghosh, Prof. Sukti Chakaraborty, and Mr. Nirmalya Chattejee taught me the beauty of life sciences.

I am glad to have relentless support from all my friends, at home and abroad. Special thanks to Soumini and Sudeshna for those long distance calls when I needed that emotional support most. I am fortunate to have friends like Chaity, Dyotana, Hridis, Pradipta, Riddhi, Soumyadyuti, Sourav, Subhadip; later--Arnab, Aswin, Deep, Partha, Roshni, Samriddhi, Shirshendu, Sirshendu, and Sohom. Special thanks to Partha for being there, come rain or shine.

I wish my uncle and grandparents were present among us to enjoy this day of fulfillment; I am dedicating this dissertation to their loving memory.

I am really grateful to Chotopishi (paternal aunt- Mrs. Rajlakshmi Biswas) and her family for their support. Special thanks to Pisha (Mr. Bimal Krishna Biswas) who has been showering his blessings throughout and is really keen on seeing me finish this dissertation. I am thankful to my extended family members as well for being there.

Finally and most importantly, I am falling short of words of appreciation for my parents- Mr. Som Nath Sarkar and Mrs. Indrani Sarkar. As I am mustering maturity, I understand the hardship you have undertaken in enabling me achieve my dreams. Above all, you taught me to be independent and self-sufficient. Thank you so much for your unwavering love and encouragement in everything I did.

Table of Contents

List of Tables

List of Figures

Chapter 1. Ligand binding studies of LFABP

1.1. Introduction

1.1.1. Importance of Fatty acids

Fatty acids (FA) are lipid molecules with polar head groups and a non-polar hydrocarbon tail of varying chain length. The general structure of fatty acids (right panel, Figure 1.1) is presented along with three representative fatty acids in Figure 1.1, left panel.

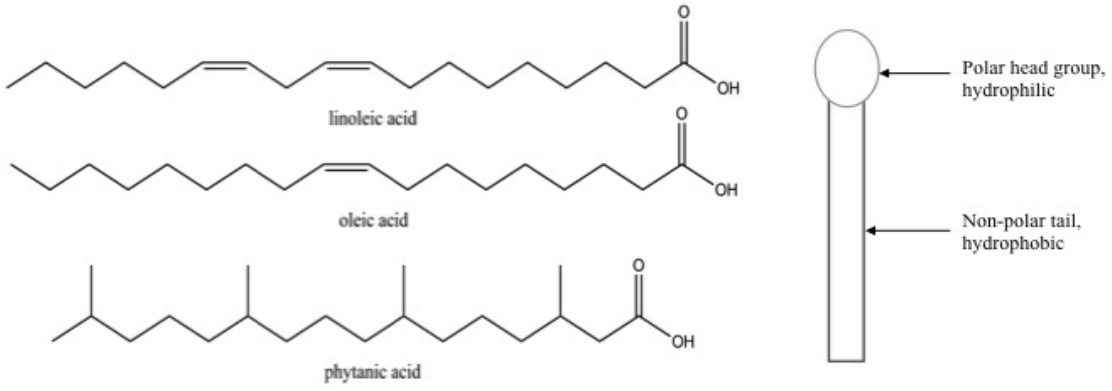

Figure 1.1. Structures of Fatty acids.

FAs are important cellular constituents taking part in various metabolic processes, for example fatty acid oxidation, fat storage in adipose tissue and other catabolic pathways. It has been hypothesized that special class of molecules, fatty acid binding proteins (FABPs) transport fatty acids with hydrophobic moieties to different cellular destinations[1].

1.1.2. Fatty acid binding proteins (FABPs)

1.1.2.1. Physiological location and function

Mammalian FABPs belong to a broad family of intracellular lipid binding proteins (iLBPs). FABPs evolved from a common ancestor as a result of gene duplication. Mammalian FABP family consists of nine different FABPs, expressed in various mammalian tissues, and cellular retinoid binding proteins[2]. The different mammalian FABPs are adipocyte fatty acid binding protein (AFABP), heart fatty acid binding protein (HFABP), intestinal fatty acid binding protein (IFABP), liver fatty acid binding protein (LFABP), keratinocyte fatty acid binding protein (KFABP), brain fatty acid binding protein (BFABP), myelin fatty acid binding protein (MFABP), ileal bile-acid binding protein and testicular fatty acid binding protein[2]. It was reported that some of them are expressed only in a single tissue, while LFABP, AFABP, HFABP are expressed in more than one location. LFABP is expressed in liver and small intestine, AFABP is expressed in adipocyte, macrophages, and HFABP is expressed in heart and brain [3].

FABPs are known to bind single molecules of long chain fatty acids (LCFAs), with the exception of liver fatty acid binding protein (LFABP), which binds two LCFA molecules and other hydrophobic ligands such as lysophospholipids, bile salts and monoacylglycerols[4]. Physiologically FABPs are known to function as fatty acid transporters to various cellular destinations[4,5], such as the endoplasmic reticulum for phospholipid and triglyceride synthesis, the mitochondria and the peroxisomes for fatty acid oxidation, and the nucleus for regulation of gene expression involved in lipid metabolism. Moreover, FABPs may also transport fatty acids to lipid droplets, whereby the fatty acids can be incorporated to phospholipid or triglyceride by acyltransferase enzymes.

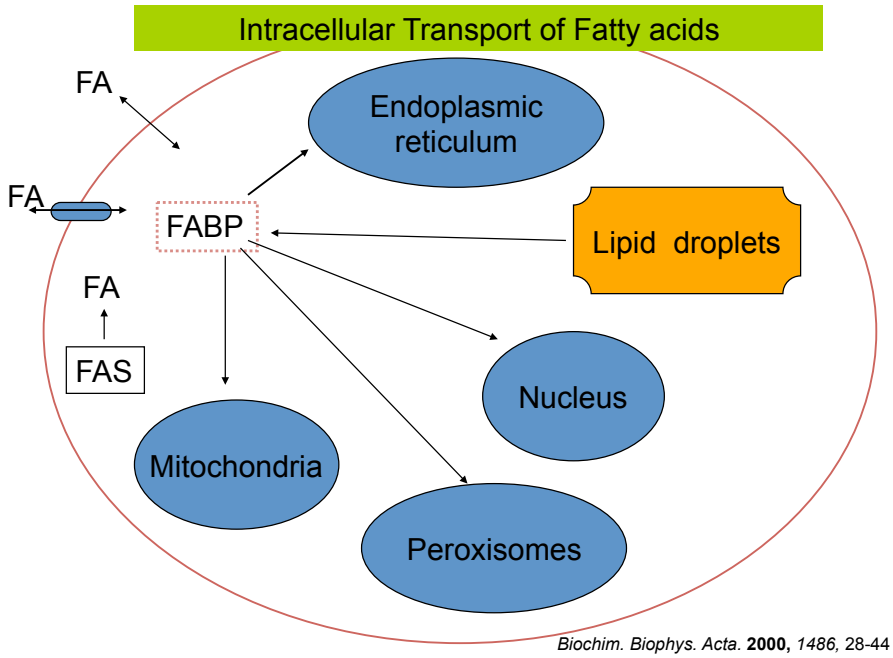

Figure 1.2. Schematic representation of the role of FABP in cellular fatty acid transport and trafficking[5].

FABPs assimilate dietary lipids in the intestine, participate in targeting liver lipids to anabolic and catabolic pathways, and aid in lipid storage in adipose tissue[4]. The main function of FABPs is to shield the hydrophobic tails of fatty acids from the aqueous environment of the cell. It has also been reported that FABPs are responsible for inter-cytosolic transport of fatty acids to the nucleus[2,6].

1.1.2.2. FABP family

a) Structural characteristics of the family

FABPs are small, cytosolic proteins of molecular weight 14kDa. The mammalian FABPs exhibit moderate (20-70%) primary sequence similarity, while they possess an astonishing tertiary structural similarity[2], shown by X-ray crystallographic[7] and NMR analyses[8,9]. Mammalian FABPs possess 10 anti-parallel β-strands and two short α-helices connecting the first and second β-strands, arranged in a so-called β-clam motif with a large internal cavity. The solvent

accessible ligand-binding cavity is centered at the end of β-barrel close to the helix-turn-helix motif, which is reported to be a portal for ligand entry and egress[10]. The β-barrel cavity is considerably larger than the ligand. Structural studies revealed presence of ordered water molecules hydrogen bonded to internal polar residues within the ligand-binding cavity[2].

b) LFABP

LFABP is a unique member of the mammalian FABP family. It exhibits 22%-27% sequence homology with FABPs from heart, adipose and myelin sheath, whereas these latter proteins are 60-65% homologous to each other[11,12]. Mainly expressed in liver, comprising 5% of liver cytosolic proteins, LFABP is co-expressed in the small intestine along with IFABP. LFABP in the small intestine has been linked to the specialized function of intestinal lipid absorption. It is the only FABP to be expressed in the liver. As noted above, LFABP can bind two LCFA and other hydrophobic ligands, such as lysophospholipids, bile salts and monoacylglycerols, compared to only one molecule of LCFA bound by other members of the family. Accommodation of two LCFA by LFABP is attributable to its large ligand-binding cavity. The mode of transport of ligands by LFABP to and from membranes is by aqueous diffusion in contrast to direct mode of collisional transfer employed by other FABP members[13,14].

Three-dimensional structures of apo and oleate liganded holo-LFABP were solved using solution state NMR[8]. The solution state NMR structure of the apo protein showed considerable conformational variability in the portal region, which is known to assist in ligand entry and exit. Three-dimensional solution state NMR structure of the holo form bound to oleate showed the internal oleate in an U-shaped conformation while the extended oleate close to the portal region exhibited multiple conformations based on computational calculations[8]. Both electrostatic and hydrophobic interactions are key factors in oleate binding in the internal cavity, in that binding is

favored by a deprotonated carboxylate but short chain fatty acids do not bind despite having a similarly charged carboxylate functional group.

It was also reported that the binding affinities of the two ligand-binding sites are comparable for saturated fatty acids, whereas the internal site exhibits a ten-fold higher affinity for unsaturated fatty acids[15].

In terms of individual ligand binding, linoleate binding to LFABP was shown to be three times weaker than oleate binding; with dissociation constant (K_d) of 29 nM for linoleate compared to 9 nM for oleate[15]. Among saturated fatty acids, phytanic acid was reported to be a ligand and transcriptional activator for LFABP[16]. Presence of methyl branches distinguishes phytanic acid from common mammalian fatty acids. For phytanic acid the dissociation constants (K_d) were reported to be 15 nM (for the first ligand-binding site) and 286 nM (for the second ligand-binding site) by isothermal titration calorimetric measurements[16]. In a separate study, fluorescence methods were used to establish that glucose binds to LFABP with a K_d of 103 nM. Reportedly, conformational changes resulting from this binding increase affinity of LFABP towards lipid ligands[17]. In accordance with diverse ligand specificity of LFABP, warfarin, a small anticoagulant drug was speculated to bind LFABP 20 times more tightly compared to oleate[18]. This observation was based on biochemical assay. However, molecular details of these reported interactions are unavailable to this date.

1.1.3. Overall objective

In this dissertation, the objective was to investigate and compare different ligand binding characteristics of LFABP including comparison of binding location and stoichiometry of binding between fatty acids with varying degrees of unsaturation using solution state NMR. Additionally, considering diverse ligand binding specificity of LFABP, warfarin and glucose were also tested

as potential ligands. The choice of these ligands was motivated by studies performed by biochemical and fluorescence methods. The rationale behind choice of ligands was to compare binding characteristics between fatty acids with varying degrees of unsaturation. So, the aim was to compare the well-established oleate (18 carbons with single unsaturation) binding with linoleate (18 carbons with double unsaturation) and phytanic acid (saturated with 16 carbons, branched chain fatty acid) binding to LFABP. Additionally, studies in this work also aimed to delineate location of warfarin binding to LFABP in comparison to oleate.

Overall, three fatty acid ligands, with varying degrees of unsaturation, and two non-lipid ligands (warfarin and glucose) were chosen to encompass a variety of reported ligands for LFABP. The structures of these ligands are presented in Figure 1.3.

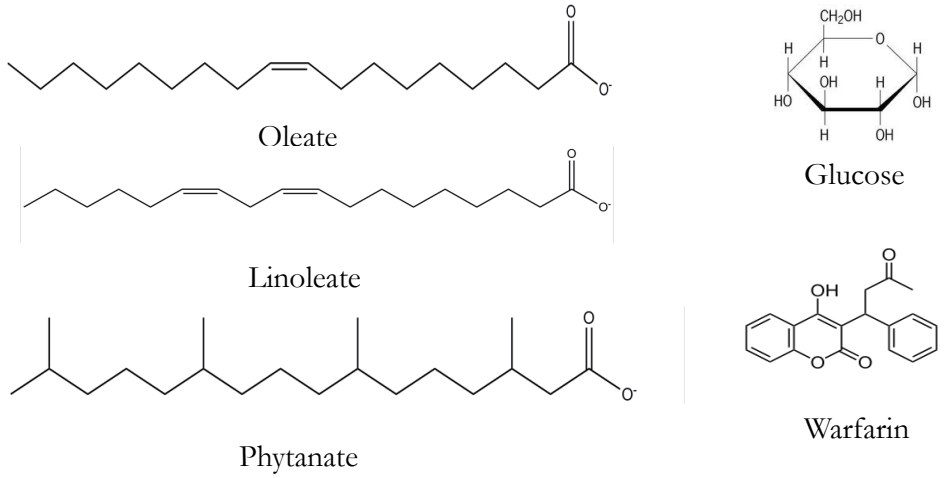

Figure 1.3. Structures of ligands studied in this dissertation.

1.1.4. NMR experiments

1.1.4.1. Two-dimensional (2D) HSQC experiment

HSQC stands for heteronuclear single quantum coherence. It is an inverse correlation experiment where the ^{1}H chemical shift is detected in the direct dimension (F2), whereas the chemical shift of the heteronucleus (^{15}N) is detected in the indirect dimension[19]. It provides a chemical shift correlation map of directly bonded ^{15}N and ^{1}H nuclei. Each peak represents a single ^{15}N-^{1}H amide of an amino acid of the protein; side chain NH_2 groups from Asn, Gln and side-chain NH from Arg, Trp and His are also visible in the spectrum.

1.1.4.2. Three-dimensional (3D) experiments

a) TOCSY-HSQC

This is a TOtal Correlation SpectroscopY where magnetization is transferred according to scalar coupling among groups of protons[19]. The magnetization transfer proceeds beyond directly bonded nuclei and reaches an extended network of scalar coupled, covalently linked spins. This experiment provides an extra dimension (^{1}H-TOCSY) to the HSQC ^{1}H and ^{15}N dimension and enables spin system identification as it correlates every proton of an amino acid with its amide nitrogen.

b) NOESY-HSQC

The Nuclear Overhauser Effect SpectroscopY experiment is based on magnetization transfer by through-space dipolar interactions between pairs of nuclei separated by less than 5Å[19]. Typically, there is an inverse sixth power dependence of the pairwise dipolar interaction and the distance between the coupled nuclei. For α-helices strong d_{NN} (i, i+1) corresponding to distance of ~2.7 Å can be observed, while weak $d_{\alpha N}$ (i, i+2), $d_{\alpha N}$ (i, i+3) and $d_{\alpha N}$ (i, i+4) can also be observed. For β-strands, strong NOE connectivity is observed for $d_{\alpha N}$ (i, i+1) and a weak NOE is sometimes

observed for d_{NN} (i, i+1). Additionally, NOEs are observed between nearby protons on adjacent β-strands in a β-sheet. This experiment provides a ^{1}H NOESY dimension to the ^{1}H and ^{15}N HSQC dimension and allows the connection of protons of different spin systems, thereby assisting in sequential resonance assignment of the protein.

c) Illustration of 3D Experiments for LFABP

Typical NOE connections (observed in NOESY-HSQC) for α-helical region E26-I35 of rat LFABP is presented in strip plot (Upper panel, Figure 1.4) and interstrand hydrogen bonding pattern observed between pairs of proton spins for nearby β-strands (βG- βJ) is presented in Figure 1.4, lower panel. The illustration (reproduced with permission from Dr. Yan He) indicates strong d_{NN} (i, i+1) and weak $d_{\alpha N}$ (i, i+1), $d_{\alpha N}$ (i, i+3) connectivities for α-helices. Strong $d_{\alpha N}$ (i, i+1) connectivities prominent throughout rat LFABP and weak d_{NN} (i, i+1) NOE (observed occasionally) are indicative of β-strands.

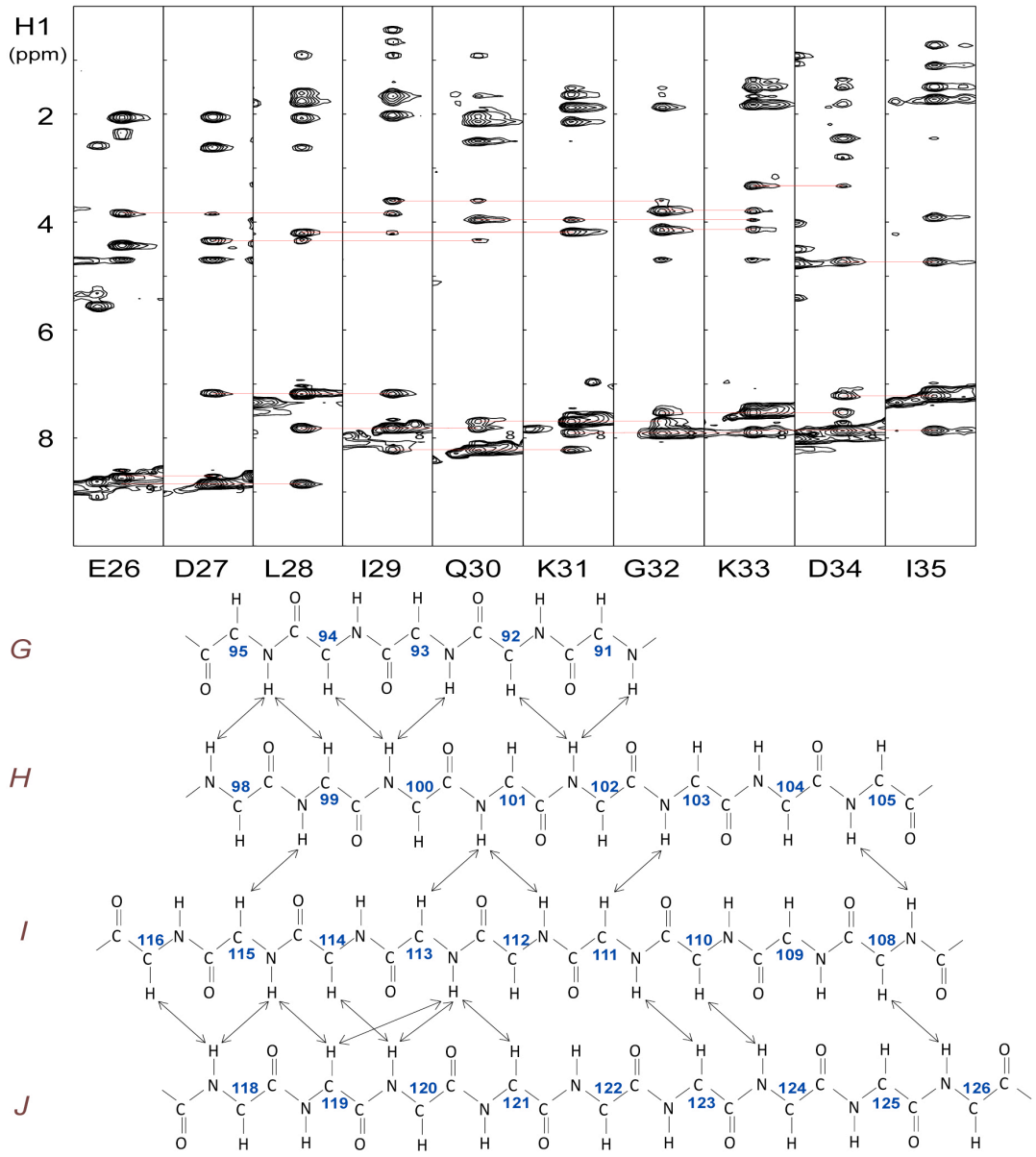

Figure 1.4. NOE connectivities observed in NOESY-HSQC of ^{15}N-LFABP.
Upper panel: strip plot for α-helical region E26-I35, lower panel: interstrand hydrogen bonding pattern between pairs of proton spins in β-strands (βG- βJ). Reproduced with permission from doctoral dissertation of Dr. Yan He.

1.2. Materials and Methods

1.2.1. Overexpression and purification of ^{15}N-LFABP

1.2.1.1. Overexpression

BL 21 (DE 3) *E.coli* cells transformed with the pET11a expression vector (kindly provided by Prof. Judith Storch, Rutgers University), containing the cDNA for LFABP and carrying ampicillin resistance, were inoculated into agar on a petri dish with ampicillin (100 μg/ml), and incubated at 37°C overnight. The following day, a single colony from the plate was transformed into 50 ml LB-agar medium containing 100 μg/ml ampicillin and incubated with shaking (200 rpm) at 37°C (pre-culture stage). Once the optical density, measured at 600 nm (OD_{600}), of the pre-culture reached 0.6, the content was transferred to a 2L LB-agar medium containing 100 μg/ml ampicillin and incubated with shaking at 200 rpm, 37°C. Once the OD_{600} of the 2L culture reached 0.6, the cells were harvested and then the pellet was resuspended in 1L minimal media (containing 100 μg/ml ampicillin) supplemented with $^{15}NH_4Cl$ (Isotech, Miamisburg, OH) for isotopic enrichment of the protein. After re-suspending the cells in minimal media, they were grown for an hour; OD_{600} was measured to ensure growth has recovered. At this stage, the culture was induced for overexpression of the LFABP gene. To induce overexpression of the LFABP gene, 4ml of 250 mM stock isopropyl-thio-galactoside (IPTG) was added to a final concentration of 1 mM and the culture was allowed to grow for another 3 hours. Finally, the cells were harvested and centrifuged (5000 rpm for 15 minutes at 4°C). The pellet was saved at -80°C for subsequent purification procedures. A 50μl aliquot was saved before and after IPTG induction to check protein expression by SDS-PAGE.

1.2.1.2. Purification

After the cell lysis step, the purification was performed in three successive steps: size-exclusion chromatography, ion exchange chromatography and delipidation.

a) Cell lysis and gel filtration chromatography

After thawing the cell pellet in an ice bath, it was completely resuspended in 25 ml lysis buffer (10 mM Tris, 1 mM EDTA, 100 mM KCl, pH 7.7 at room temperature). Prior to adding the cell pellet, 25µl of PMSF (Phenylmethylsulfonyl fluoride) with a stock concentration of 100 mM was added to the lysis buffer as a protease inhibitor. The resuspended cell pellet was sonicated (55% duty cycle, 30 seconds pulse on, 1 min resting period) 8-12 times in an ice-bath. Following sonication, the cell lysate was centrifuged at 19000 rpm for 45 minutes at 4°C, to get rid of the cellular debris and to release LFABP into the supernatant. Considering that the typical yield of LFABP is 30 mg per liter of culture[8] and the molecular weight of LFABP is 14.5 kDa, an excess of the oleate ligand was added to the supernatant, at a protein: ligand molar ratio of 1:3, to ensure proper folding of LFABP (J. Storch, personal communication). This supernatant-oleate complex was incubated on a rocker at room temperature for 30 minutes and then loaded on a pre-equilibrated gel filtration column that was pre-washed with potassium chloride phosphate buffer (150 mM KCl, 10 mM phosphate, 0.02% sodium azide, pH 7.4). The flow rate was fixed at 1ml/min. After flushing the column with one column volume (600 ml) of buffer (the largest impurities were eluted) as presented by the SDS-PAGE in Figure 1.5. Then, fractions were collected with an automated fraction collector set at 8min/fraction. The entire procedure was performed at 4°C. At the end of fraction collection, the UV/Vis absorbance was measured for alternate fractions at 280 nm and SDS-PAGE was performed in order to identify the fractions containing LFABP. The corresponding fractions were then concentrated ten times by

ultrafiltration, using a membrane with a molecular weight cut-off of 5 kD (Milipore, #PLCC06210, Billerica, MA), for further purification by ion-exchange chromatography.

b) Ion-exchange chromatography

Anion exchange chromatography was used as the next step to isolate LFABP. Pre-swollen Diethylaminoethyl cellulose (DE 52) beads were washed with 10 mM Tris buffer (with 0.02% sodium azide, as a bactericidal agent), pH 8.3 at 4°C, until the pH was stabilized at a constant value of 8.3 at 4°C. Typically, it took six column volumes of buffer (~2000 ml) to stabilize the pH at 8.3 (4°C). LFABP came out of the column right away despite an opposite expectation based on its isoelectric point of 7.0[20], while the contaminants remained bound to the column. 80 fractions were collected at a flow rate of 1ml/min. It has been observed that by the 80th fraction the absorbance value reaches the baseline level. After inspecting the UV/Vis absorbance profile, fractions were chosen to perform SDS-PAGE. SDS-PAGE (Figure 1.6) showed that further purification was achieved by ion-exchange chromatography. Then, fractions with LFABP were pooled and concentrated by ultrafiltration for subsequent delipidation procedures.

c) Delipidation to remove endogenous lipids from LFABP

Hydroxyalkoxypropyl-dextran type-VI (equivalent to Lipidex 1000) beads were used for this procedure. The regenerated beads stored in 100% methanol were washed with a decreasing (100%, 50%, 30% and 15%) gradient of methanol and finally equilibrated in potassium chloride phosphate buffer (150 mM KCl, 10 mM phosphate, 0.02% sodium azide, pH 7.4). The beads were packed into the pre-heated column at 37°C and washed with potassium chloride phosphate buffer at a flow rate of 2.8 ml/min for 3 hours. After the beads were uniformly packed, the concentrated oleate-bound LFABP sample was loaded onto the column to remove the bound fatty acid from the protein, since the hydrophobic beads would attract the lipid strongly. During

the delipidation process the flow rate was fixed at 0.29 ml/min; 50 fractions were collected with the fraction collector adjusted to 9 min/fraction. By observation of NMR spectral features (as discussed later in results, Section 1.3) and prior trials with radioactive oleate[8,21], it was decided that LFABP would need two successive delipidation procedures to strip off oleate ligand completely. After completing the delipidation procedure, SDS-PAGE was performed to identify the fractions containing LFABP.

1.2.2. NMR experiments

1.2.2.1. NMR sample preparation

Delipidated fractions containing LFABP were pooled, concentrated and exchanged into the buffer (100 mM KCl, 50 mM KH_2PO_4, 5μM EDTA, 0.02% NaN_3, pH 7.0) conventionally used for NMR experiments. The desired concentrations for acquisition of two-dimensional (HSQC) and three-dimensional (TOCSY-HSQC, NOESY-HSQC) NMR spectrum are in the range of 0.1-0.3 mM and 0.4-0.8 mM respectively. Concentration was determined using Nanodrop (Wilmington, DE) with 6400 M^{-1} cm^{-1} as the molar absorption coefficient of LFABP[7]. 5% by volume D_2O was added to 500 μl NMR sample for a ^2H lock signal and it was put into a 5mm NMR tube.

1.2.2.2. 2D ^{15}N HSQC

^{15}N-HSQC spectra were recorded using a Varian four-channel spectrometer with ^1H frequency at 600 MHz (conventional probe). In specific cases, a Varian instrument with cryoprobe was also used. Alternatively, a Bruker four-channel spectrometer with cryoprobe was used. ^{15}N-HSQC spectra were recorded with 1024 points in the direct dimension, 256 points in the indirect dimension and with 32 transients, unless otherwise mentioned. The data were processed with

NMRpipe software[22], with typical parameters as shown in Table 1.1 and analyzed with NMRViewJ[23].

nmrPipe -in test.fid	\.*Format Input*
| nmrPipe -fn SOL -fl 32	*solvent filter*
| nmrPipe -fn SP -off 0.35 -end 1.00 -pow 2 -c 0.5	*Window*
| nmrPipe -fn ZF –auto	*Zero-fill*
| nmrPipe -fn FT –auto	*Fourier-transform*
| nmrPipe -fn PS -p0 41.00 -p1 0.00 -di –verb	*Phase, delete imaginaries*
| nmrPipe -fn POLY -auto -ord 0	*Auto-baseline correct*
| nmrPipe -fn EXT -left –sw	*Extract the left half*
| nmrPipe -fn TP	*Transpose X/Y*
| nmrPipe -fn LP -x1 1 -xn 64 -ord 10 -f -pred 64 –after	*Linear prediction*
| nmrPipe -fn SP -off 0.35 -end 1.00 -pow 2 -c 0.5	*Window*
| nmrPipe -fn ZF –auto	*Zero-fill*
| nmrPipe -fn FT –alt	*Fourier transform*
| nmrPipe -fn PS -p0 0.0 -p1 0.00 -di –verb	*Phase correct, delete imaginaries*
| nmrPipe -fn TP	*Transpose X/Y*
| nmrPipe -fn POLY -auto -ords 0	*Auto-baseline correct*
-ov -out test.dat	*Format output*

Table 1.1. Annotated conversion script used for HSQC spectrum recorded in Bruker 500 spectrometer at pH 7.0, 283K.

1.2.2.3. Double resonance experiments and NMR assignment of LFABP

a) Three-dimensional TOCSY-HSQC and NOESY-HSQC

TOCSY-HSQC and NOESY-HSQC data were acquired for confirming backbone resonance assignments of apo and oleate liganded holo-LFABP with 1024 complex points in t_1, 256 complex points in t_2 and 128 complex points in t_3 and 32 transients using a four-channel Bruker 500 MHz spectrometer with a cryoprobe. Similar experiments were recorded for backbone resonance assignments of the warfarin-oleate-LFABP complex.

1.2.2.4. Titration followed by NMR

^{15}N-HSQC experiments were recorded with sequential addition of specific ligand solutions (oleate, linoleate) into apo-LFABP at 10°C. Typically, aliquots of a 2 mM stock solution of sodium oleate at pH 9.0 were added to 0.14 mM apo-LFABP in 100 mM KCl, 50 mM KH_2PO_4, 5µM EDTA, 0.02% NaN_3, pH 7.0 buffer. The titration points recorded were 1:0.26 1:0.5, 1:0.65, 1:0.78, 1:0.9, 1:1.16, 1:1.68, 1:1.95, 1:2.97 and 1:4 equivalent of protein: ligand. At the end of the titration series, the dilution factor was 1.13 times owing to the addition of aliquots of ligand solution.

In case of linoleate, a pH 9.0, 1 mM stock solution was used and the titration points recorded were 1:0.08, 1:0.17, 1:0.25, 1:0.42, 1:0.6, 1:0.77, 1:0.94, 1:1.3, 1:1.6, 1:1.97, 1:2.5, 1:3 with similar pH and temperature as oleate. At the end of the titration series the dilution factor was 1.12 times owing to the addition of aliquots of ligand solution.

For warfarin, the titration series, presented herein, started with holo-LFABP liganded with 2 equivalents of oleate. 10 mM warfarin dissolved in sodium hydroxide was used to record HSQC spectra of 0.4, 0.8, 1.2, 1.6, and 2 equivalents of added warfarin to holo-LFABP complex.

For a trial with phytanic acid, starting with apo-LFABP, 3 equivalents were added from 5mM solution of isomers of phytanic acid in NaOH and HSQC spectrum was recorded.

For glucose, excess of glucose (10 equivalents) 10 mM aqueous solution was added to apo-LFABP and HSQC spectrum was recorded.

1.2.2.5. Chemical shift perturbation analysis

Upon sequential addition of ligand solution to ^{15}N-LFABP NMR samples, the HSQC peaks of certain residues of the apo-protein spectrum may be perturbed due to a change in the chemical environment as a consequence of the interaction of the protein with the ligand. This chemical

shift perturbation (in ppm) was calculated using the formula $[(\delta_H apo\text{-}\delta_H holo)^2 + \{(\delta_N apo\text{-}\delta_N holo)/6.51\}^2]^{1/2}$, where δ_H is the proton chemical shift, whereas δ_N is the nitrogen chemical shift[24].

1.3. Results

1.3.1. Overexpression and purification

SDS-PAGE migration analysis of the overexpression and subsequent purification of LFABP by gel filtration chromatography is presented in Figure 1.5.

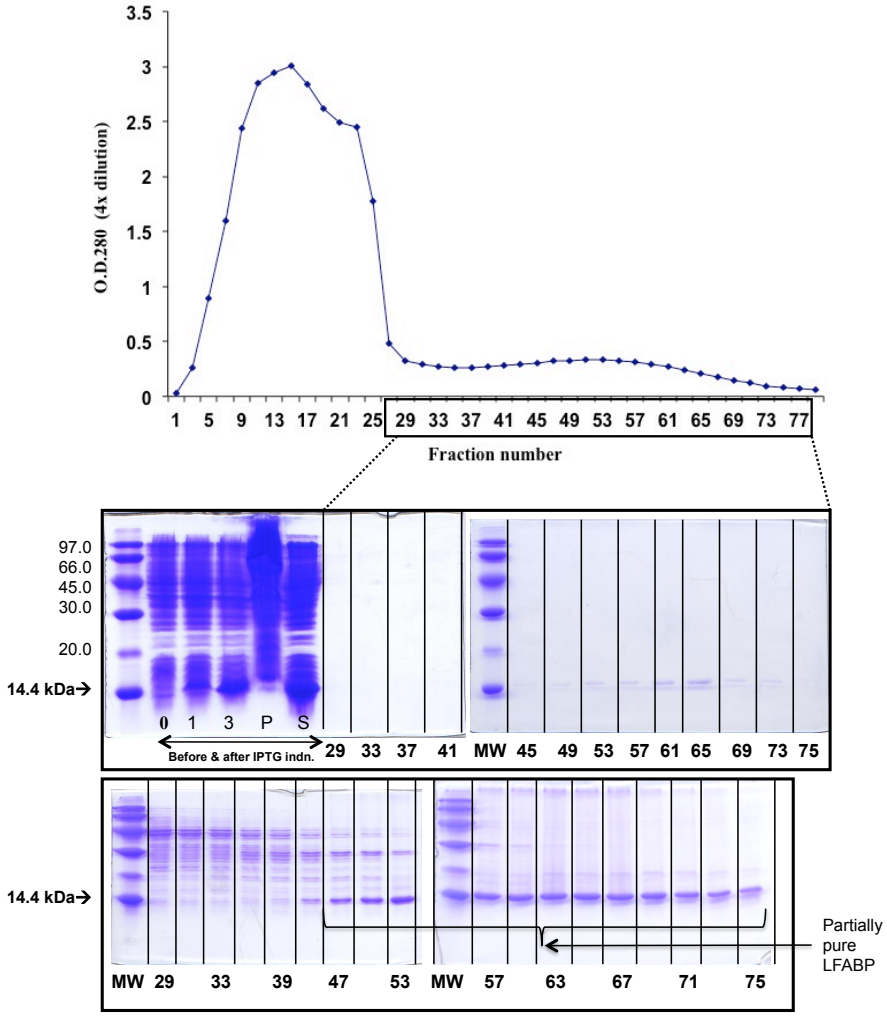

Figure 1.5. Gel filtration chromatographic purification of ^{15}N-LFABP monitored by SDS-PAGE.

Uppermost panel: Elution profile showing absorbance measured at 280 nm vs. fraction number;

Middle panel (left): SDS PAGE migration analysis of LFABP overexpression (0, 1, 3 refer to number of hours after IPTG induction), solubility.

Remaining lanes represent protein content of eluted fractions 29-75 diluted 4 times, (middle panel, right) and diluted twice (lower panel).

From the gel, it is clear that protein is overexpressed (lanes 0, 1, 3). Comparing the pellet (P) and the supernatant (S), it is observed that protein of interest is in the soluble fraction. Also, the protein band is absent in the insoluble fraction (P, pellet) and present in the soluble fraction (S, supernatant). From the lanes (29-75) of protein samples, it is clear that LFABP is isolated from most of the proteins of different size. Also, comparing the panel of gels, it appears clearly that better band density is achieved by using 2x-diluted sample (lower panel of gels) compared to 4x-diluted samples (middle panel, right).

After analyzing the elution profile of LFABP by gel filtration chromatography, fractions 47-75 were pooled and concentrated by ultrafiltration and the resulting concentrate was subjected to ion exchange chromatography. Analysis of anion exchange chromatographic fractions of LFABP is presented in Figure 1.6. Compared to the pooled fractions after gel filtration (middle panel, left, lane 2, marked G50) LFABP is well isolated from all other proteins with an acceptable purity (the samples were not diluted for migration and it is clear that LFABP is almost completely pure). All the remaining proteins were eluted with 1M KCl (middle panel: right and lower panel), where LFABP is not present.

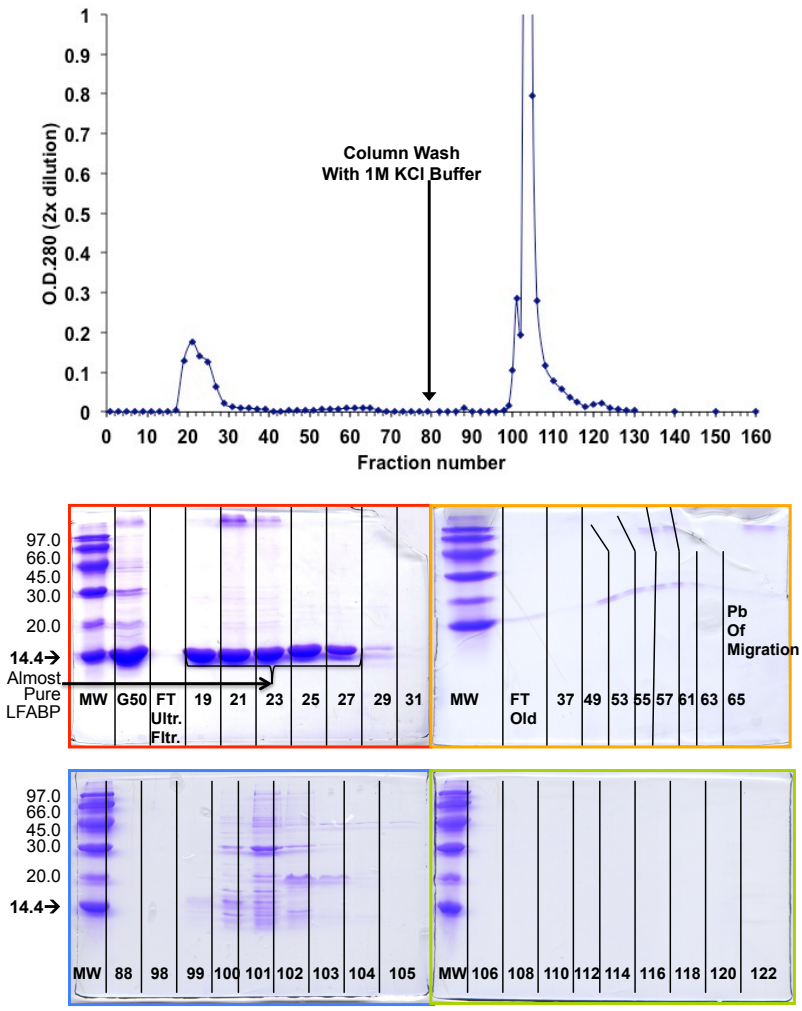

Figure 1.6. Anion exchange chromatographic purification of ^{15}N-LFABP monitored by SDS-PAGE.

Uppermost panel: elution profile of protein, middle & lower panel: gels of protein samples.

Middle panel (left) lane 2 marked G50: pooled fractions of gel filtration, lane 3, marked FT: Flow through from ultrafiltration and remaining lanes (in middle and lower panel): migration profile of eluted fractions.

Note: there was problem during the migration of the gel on the middle right panel (Pb of migration).

After anion exchange chromatography, fractions 17-29 were pooled and concentrated for subsequent delipidation procedures. From this pool, a sample was prepared to check spectral quality by recording a ^{15}N-HSQC (Figure 1.7) experiment before delipidation. The ^{15}N-HSQC spectrum of LFABP, recorded after ion exchange chromatography (before delipidation), exhibits well-resolved peaks of uniform shape and intensity, which is indicative of a well-folded state of the protein in presence of oleate ligand. This spectrum also indicates good signal/noise ratio.

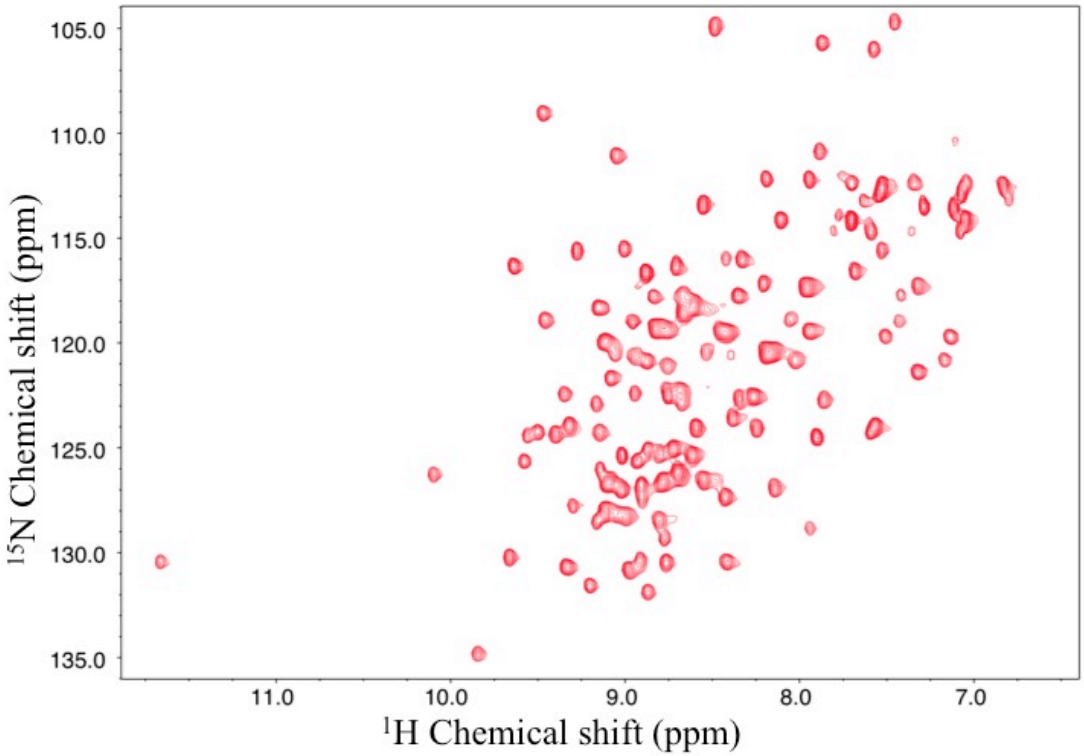

Figure 1.7. HSQC spectrum of ^{15}N-LFABP before delipidation (283K) with 32 transients.

1.3.2. Delipidation of LFABP

Following anion exchange chromatography, a delipidation step was performed to remove the oleate bound to the protein. Observing the UV absorbance and SDS-PAGE migration profile of LFABP after delipidation (Figure 1.8), it is clear that LFABP was recovered with considerable efficiency. Also, 85-90% protein mass was recovered at the end of the delipidation. Concentration measurements were based upon OD_{280}, again using 6400 $M^{-1}cm^{-1}$ as the molar absorption coefficient of the protein[7].

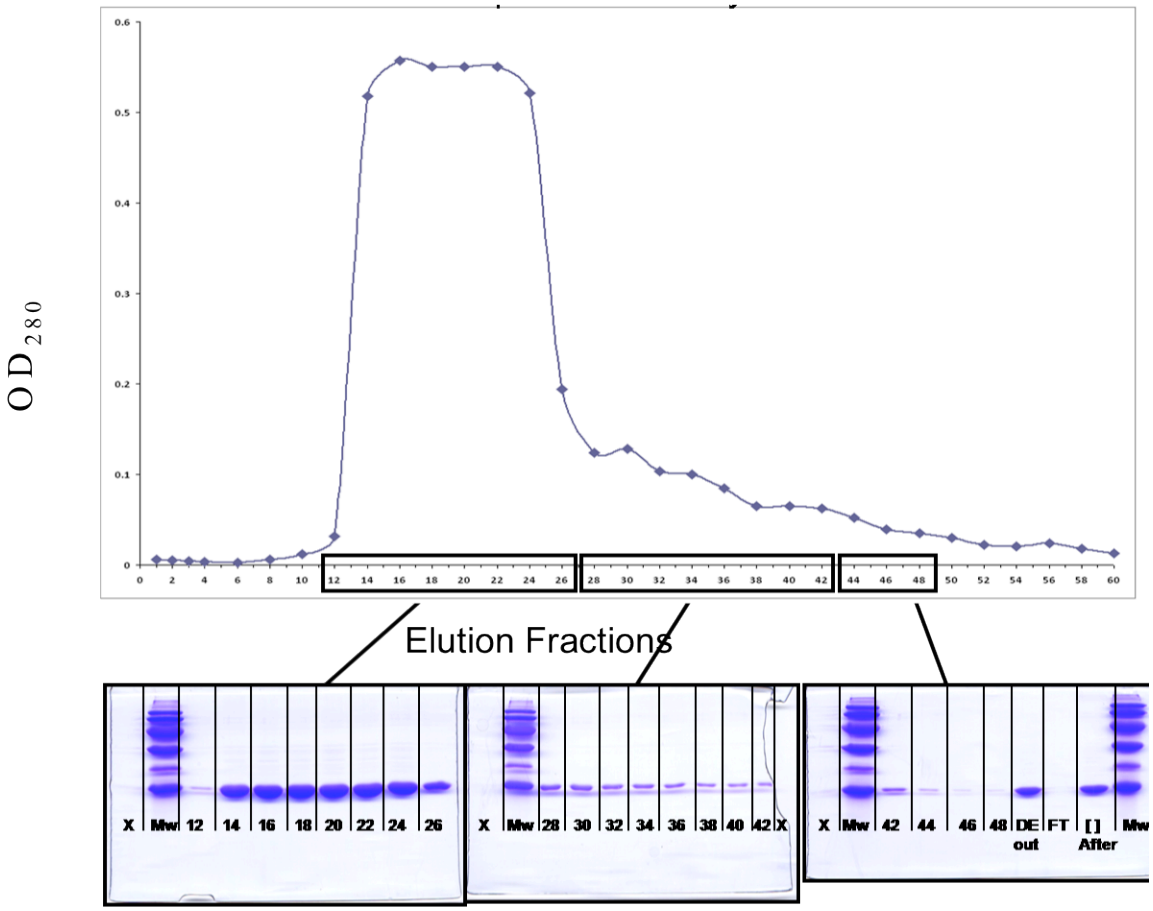

Figure 1.8. OD_{280} absorbance profile of ^{15}N-LFABP after delipidation (upper panel) and SDS-PAGE migration profile (lower panel).
The lane, DE out, indicates protein sample right after ion exchange and [] after lane indicates sample after concentration by ultrafiltration.

Comparing the ^{15}N-HSQC spectrum of LFABP before delipidation (Figure 1.9 left panel, black spectrum) and at once delipidated state (Figure 1.9, left panel, red spectrum), it appears that the two spectra exhibit some differences in chemical shifts as well as in uniformity and shape of peaks. This suggests that delipidation did remove lipids from LFABP. Earlier, by following the course of delipidation by using tritiated oleate until the scintillation count reached baseline level, it was established that two steps of delipidation are required to completely remove oleate from LFABP. ^{15}N-HSQC spectra collected after the first delipidation (Figure 1.9 right panel, red

spectrum) and after the second delipidation (apo state of the protein, green) are overlaid in the right hand panel of Figure 1.9.

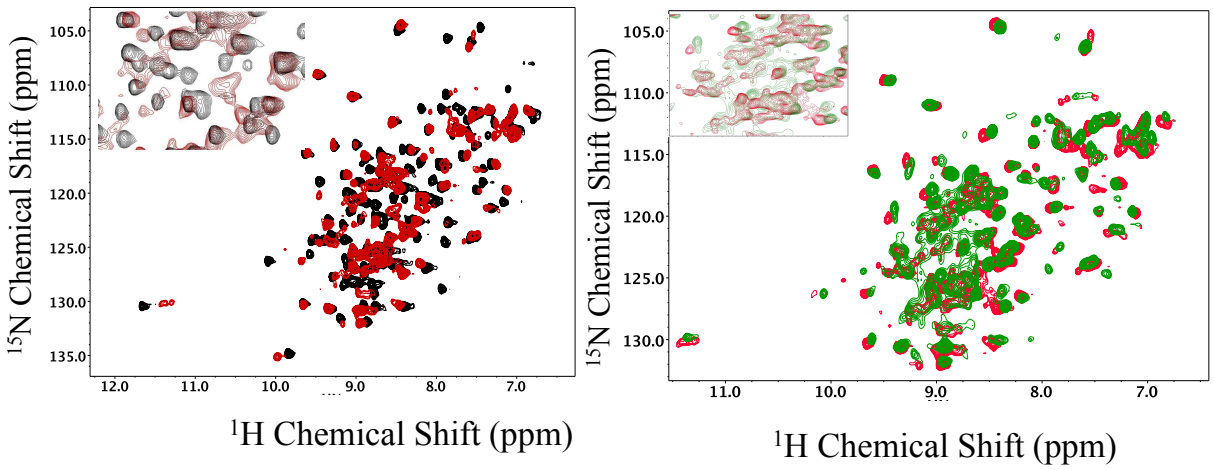

Figure 1.9. Monitoring delipidation process by HSQC experiment.
Left panel: overlay of undelipidated (black) and once delipidated (red) HSQC spectra, Right panel: overlay of once delipidated (red) and twice delipidated (green) HSQC spectra.

^{15}N-HSQC of once delipidated LFABP (Figure 1.9, right panel, red spectrum) still exhibits peak intensity and uniformity, whereas after second delipidation, in the apo state, the protein exhibits poor spectroscopic resolution (Figure 1.9, right panel, green spectrum), making resonance assignment of the peaks a difficult task.

1.3.3. Discussion

At the end of the purification process, 40 mg/l of LFABP was obtained on average. It is also noteworthy that typically 85-90% of the protein mass was recovered at the end of the delipidation procedure, according to UV/Vis absorbance measurements. As noted above, it is known from prior delipidation of LFABP monitored by scintillation counts of tritiated oleate, that two rounds of delipidation are usually required for LFABP. However, after the second delipidation, HSQC spectral features indicate major structural change leading to irregular peak intensity, overlapped peaks and spectral crowding. This makes resonance assignment of the

spectrum a daunting task and compromises subsequent chemical shift perturbation analyses. It should also be noted that the apo protein exhibited this kind of poor spectral resolution contrary to previously published results[8], wherein a single set of well resolved peaks were observed for the protein backbone. Due to this reproducibility problem for the ^{15}N-HSQC spectrum of the apo protein, the ligand binding studies (discussed in the next section, results 1.3.4.1) will be given a qualitative treatment.

1.3.4. NMR study of the interaction of LFABP with various ligands

1.3.4.1. Titration with oleate

Resonance assignments have been confirmed for 87% of the residues for apo-LFABP and 95% for the holo-LFABP, protein: oleate molar ratio of 1:4.5 (courtesy: Dr. Bernard).

By comparing the published (Figure 1.10, left panel, black) apo-LFABP HSQC spectrum with the apo-LFABP HSQC spectrum recorded during this series of experiments (Figure 1.10, left panel, red), strong differences can be observed in terms of peak positions and shape. Considerable spectral crowding was observed for the current batch of apo-LFABP spectrum.

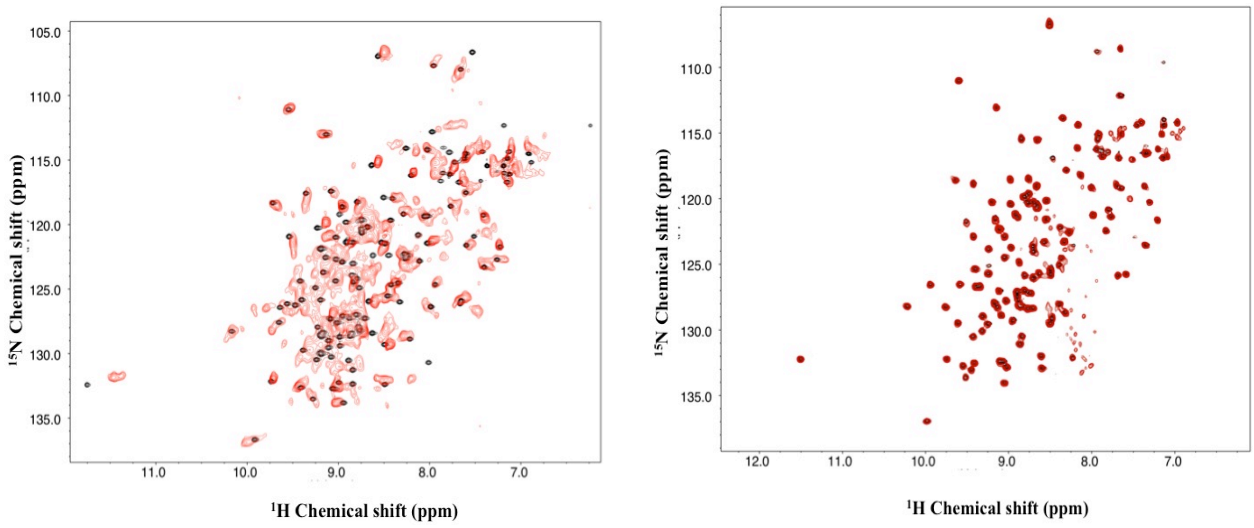

Figure 1.10. Superimposed HSQC spectra of published (black) and current (red) batch of LFABP. Left panel: superimposition of apo spectra, right panel: superimposition of holo spectra.

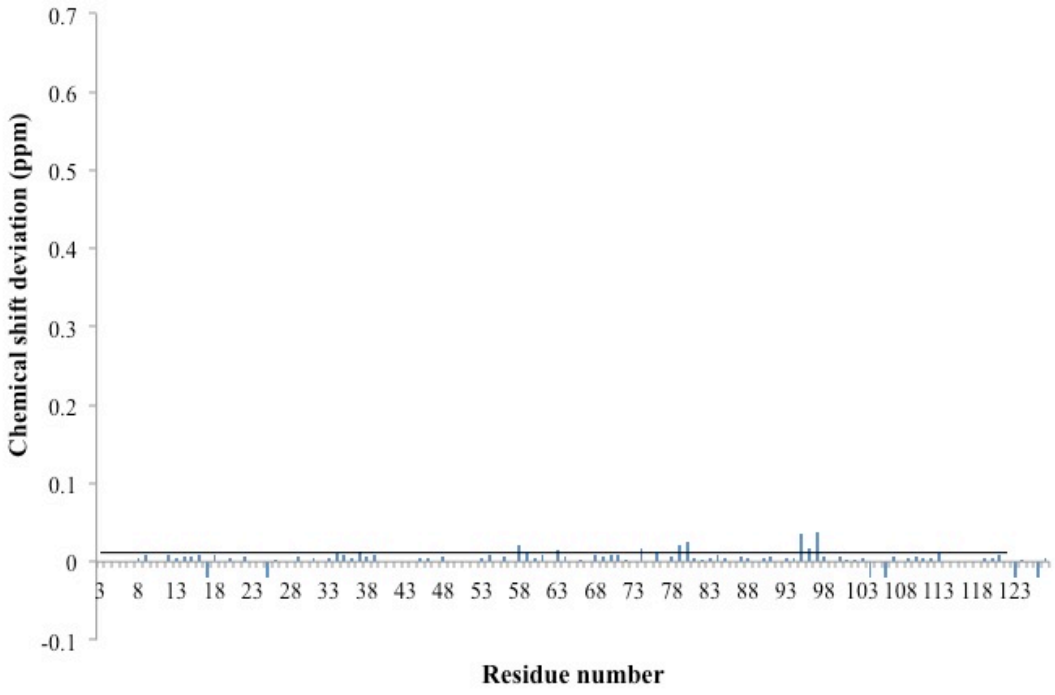

Figure 1.11. Plot of chemical shift deviation versus residue number between previous and current LFABP samples.
Comparison of holo-LFABP samples, where the black line indicates summation of standard deviation and average. Negative values indicate unassigned residues.

However, when comparing the holo form of the protein between two batches (Figure 1.10, right panel) minimal differences were observed on the overlay of the HSQC spectra of the holo proteins. This fact is illustrated with the calculation of the chemical shift deviation between the two batches of holo proteins (Figure 1.11). It is striking that although the apo proteins appear to be significantly different, the holo states of the same protein are very similar.

A chemical shift deviation plot between the apo and holo forms is presented in Figure 1.12. It is noted that the most perturbed residue is apolar G37 in the published results with chemical shift deviation of 1.13 ppm, whereas in case of the present batch, basic H60 exhibited the highest chemical shift deviation with a value of 0.866 ppm.

The magnitude of chemical shift deviation was normalized to the most perturbed residue in each case, G37 for published results and H60 for the present batch.

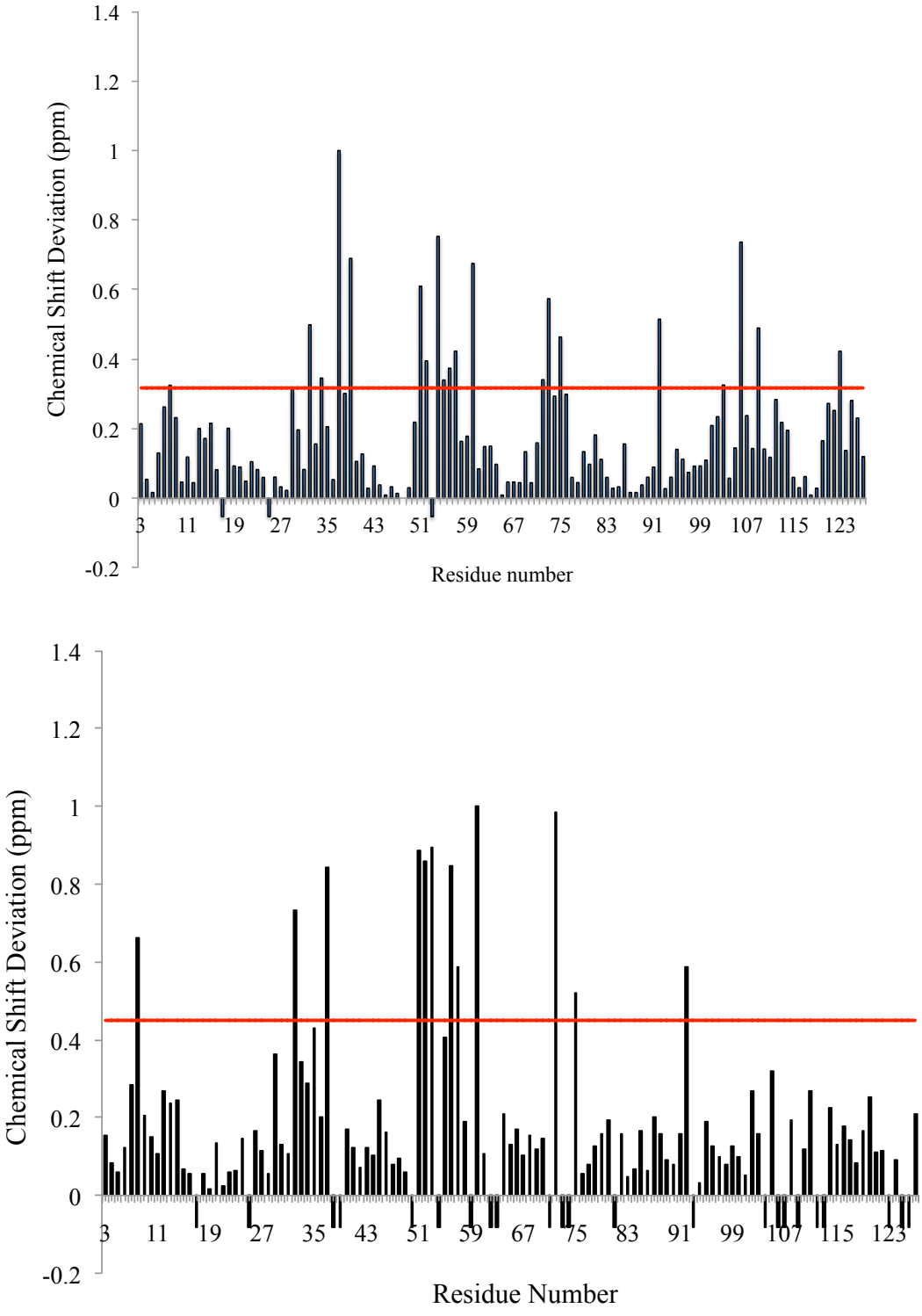

Figure 1.12. Chemical shift deviation between apo and holo LFABP mapped versus residue number normalized to most perturbed residue.
Upper panel: published results normalized to G37, lower panel: new batch, normalized to H60. Negative values indicate unassigned residues. In both panels, the red line represents the summation of average and one standard deviation: 0.32 and 0.45 ppm for previously published results and the new batch respectively.

In the case of the published results, 19 residues (Q8, G32, D34, G37, S39, T51, I52, Y54, G55, S56, K57, H60, E72, T73, T75, V92, G106, I109 and V123) exhibited significant chemical shift deviation between apo and holo form (Figure 1.12, upper panel). In comparison to the 19 residues in the published results, chemical shift deviation between apo and holo forms of the current batch is less pronounced in terms of number of residues perturbed; with only 12 residues (Q8, G32, G37, T51, I52, T53, S56, K57, H60, E72, T75 and V92) showing significant chemical shift perturbation (Figure 1.12, lower panel). From Figure 1.12, residues exhibiting significant chemical shift perturbation were mapped onto the three-dimensional NMR structure of LFABP (Figure 1.13) using PyMOL for both the previously published and new data.

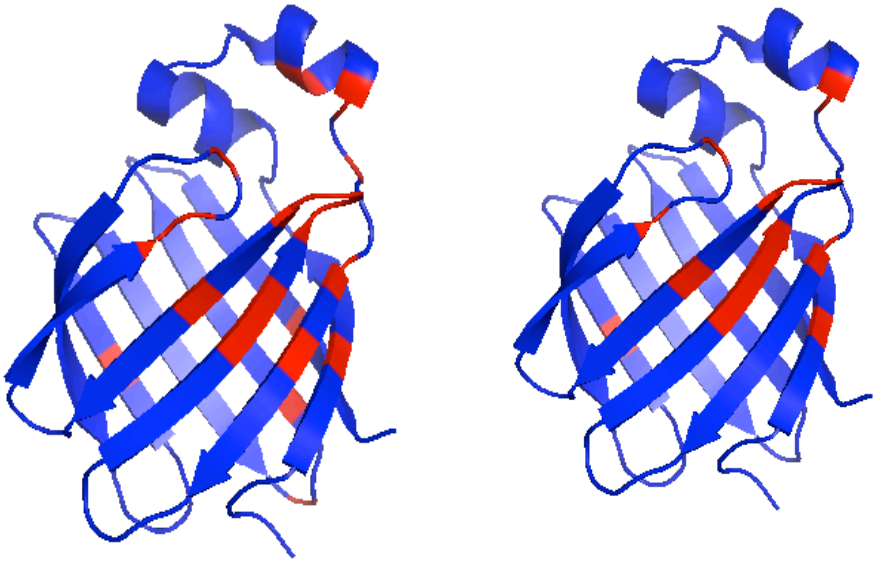

Figure 1.13. Chemical shift perturbation mapped on the structure.
Residues that are significantly perturbed upon ligand binding are indicated in red. Left: published data, right: present batch.

From this mapping, a similar observation for both batches was that apart from G32 on helix II, all the other residues, namely: Q8, G37, T51, I52, T53, G55, S56, K57, H60, E72, T75 and V92 are in the ß-barrel forming cavity. In contrast to the previously published results, residues D34, S39, Y54, G55, G106, I109, V123 are not significantly perturbed in the present batch. In spite of fewer residues perturbed in the new batch, the location of perturbation is similar in both cases.

The difference in chemical shift deviation between apo and holo of both batches can be quantified in terms of absolute value (Δ(Δδ) ppm) and is presented in Figure 1.14. By comparing the chemical shift difference of apo and holo between both batches, residues Q8, T51, I52, S56, H60, E72 and G76 exhibited a (Δ(Δδ) ppm) value above 0.24 ppm.

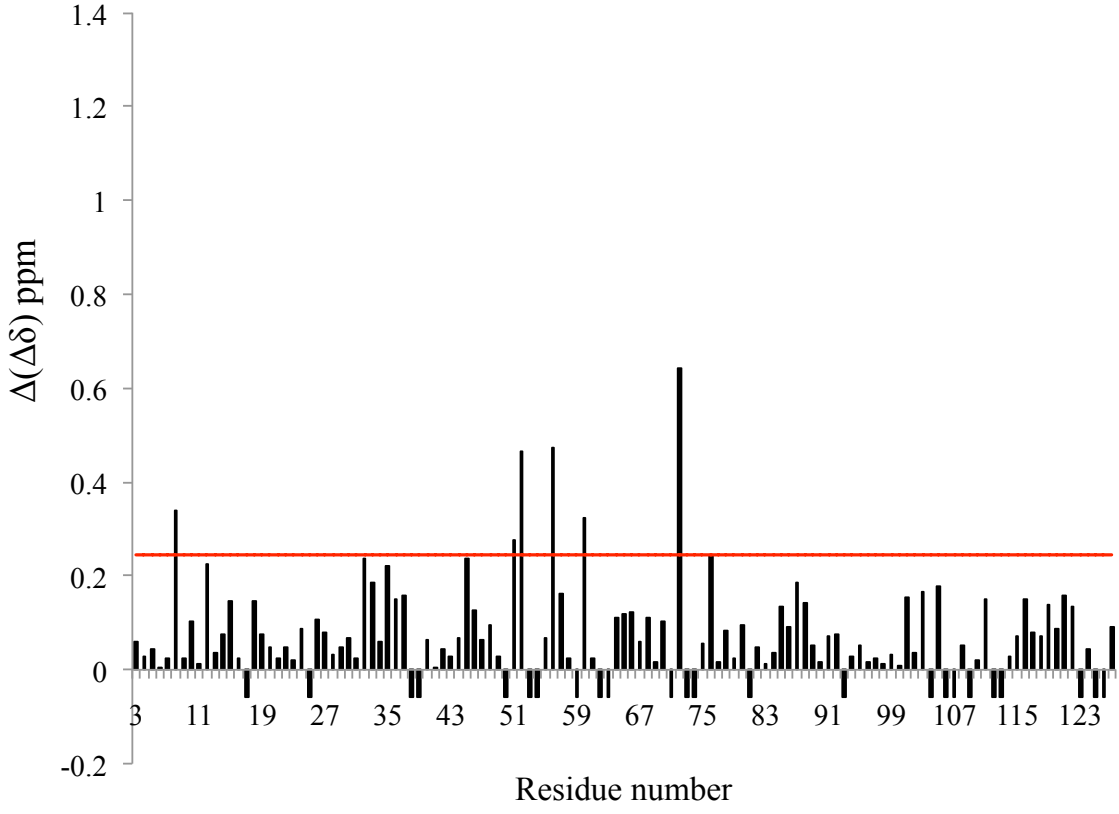

Figure 1.14. Difference of chemical shift deviation between two batches of apo and holo presented in absolute value.
Red line represents summation of average and one standard deviation. Negative values indicate unassigned residues.

In spite of the strong differences observed with apo form, the HSQC spectrum of holo form of the protein is extremely similar to the published results with minimal differences. Therefore, it is rational to attribute the observed differences in apo and holo chemical shift deviations, between the two batches, to the non-uniform apo-LFABP spectrum. In spite of the reproducibility issue of the apo form of the protein, the holo form can be compared with analogous LFABP samples in the presence of other ligands, as discussed in subsequent sections.

1.3.4.2. Titration with linoleate

A 1 mM stock solution of linoleate was added in 2µl aliquots to 0.2 mM apo-LFABP in 100 mM KCl, 50 mM KH_2PO_4, 5µM EDTA, 0.02% NaN_3, pH 7.0 buffer. The titration points started with a 1:0.2 molar ratio of protein: linoleate, going up to a 1:3 protein: linoleate ratio. ^{15}N-HSQC spectra were recorded with 1024 points in the direct dimension, 256 points in the indirect dimension and with 32 transients.

Owing to substandard HSQC spectrum of apo-LFABP with overlapped peaks of non-uniform shape, chemical shift perturbation of linoleate binding to the apo protein could not be delineated quantitatively. Therefore, discussion of linoleate binding is restricted to the 1:3 (protein: ligand) complex. The holo form (1:3 molar ratio of protein: ligand) saturated with linoleate resembles that of oleate liganded holo (1:3 molar ratio of protein: ligand) substantially, with a few residues that are differentially perturbed according to the choice of ligand. Figure 1.15 represents overlaid HSQC spectra of LFABP with bound oleate (blue) and bound linoleate (red); a close comparison is shown in inset.

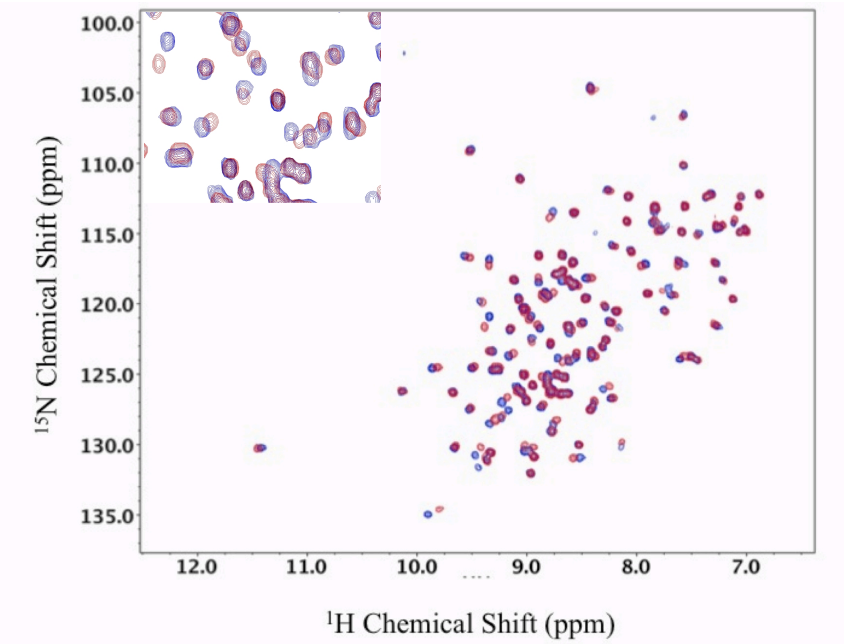

Figure 1.15. Overlaid HSQC spectra of oleate bound (blue) and linoleate bound (red) LFABP.

To account for the residues perturbed differentially for each ligand, a composite chemical shift perturbation was calculated and plotted along the sequence (Figure 1.16). In terms of magnitude of chemical shift deviation between the two ligands, residues N14, I35, V38, G55, S56, K57, I59, H60, M74, V83, V92, T93, N111, M113 and R122 exhibit chemical shift deviation of more than 0.06 ppm (summation of standard deviation and average) indicated by a red line in Figure 1.16. Among these residues, V92 and T93 exhibit the most differences between the two ligand bound states with values of 0.12 ppm and 0.15 ppm, respectively. This suggests, that the majority of chemical shift deviation variation is restricted to mainly hydrophobic and uncharged residues, with the exception of K57 (0.06 ppm) and R122 (0.06 ppm). Overall, it is clear that the differences in chemical shift perturbation are moderate between oleate and linoleate binding indicating moderately different binding location for the two ligands.

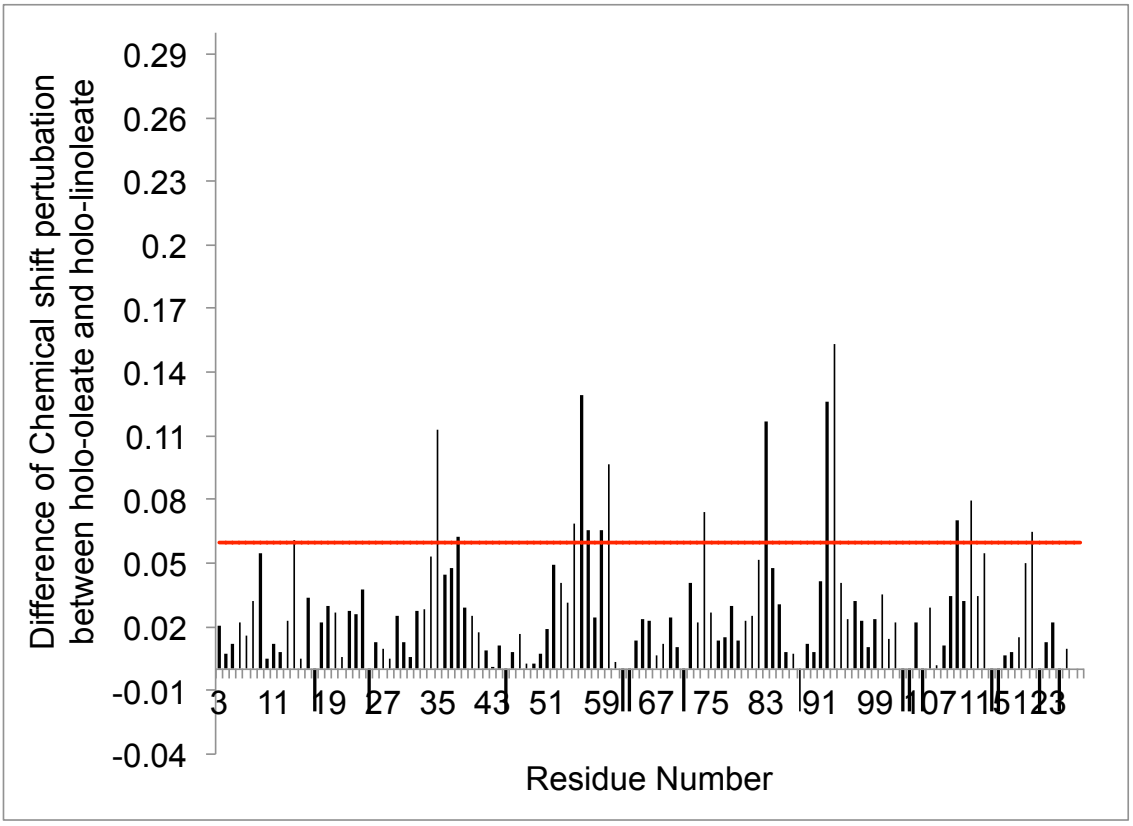

Figure 1.16. Difference of Chemical shift perturbation between oleate and linoleate liganded LFABP. The red line represents summation of average and one standard deviation. Negative values indicate unassigned residues.

To visualize the location of chemical shift perturbation by the two ligands oleate vs linoleate on LFABP, the composite chemical shift perturbation was mapped on the three dimensional solution-state NMR structure of oleate liganded LFABP as a color gradient from yellow to red in Figure 1.17. Two distinct regions on LFABP show differences in chemical shift perturbation between the binding of oleate and linoleate.

These two regions correspond to the two binding sites of the ligand: for the first ligand (shown in blue sticks), region 1 encompasses residues V83, V92, T93, N111, M113 and R122. For the second ligand (shown in green sticks), region 2 contains residues N14, I35, V38, Y54, G55, S56, K57, I59, H60, M74. These observations indicate that the orientations of oleate and linoleate have limited differences in the first binding site (due to the dimension of the cavity) with few

residues perturbed differentially according to choice of ligand, whereas in the second binding site they seem to adopt a significantly different orientation encompassing a greater number of residues.

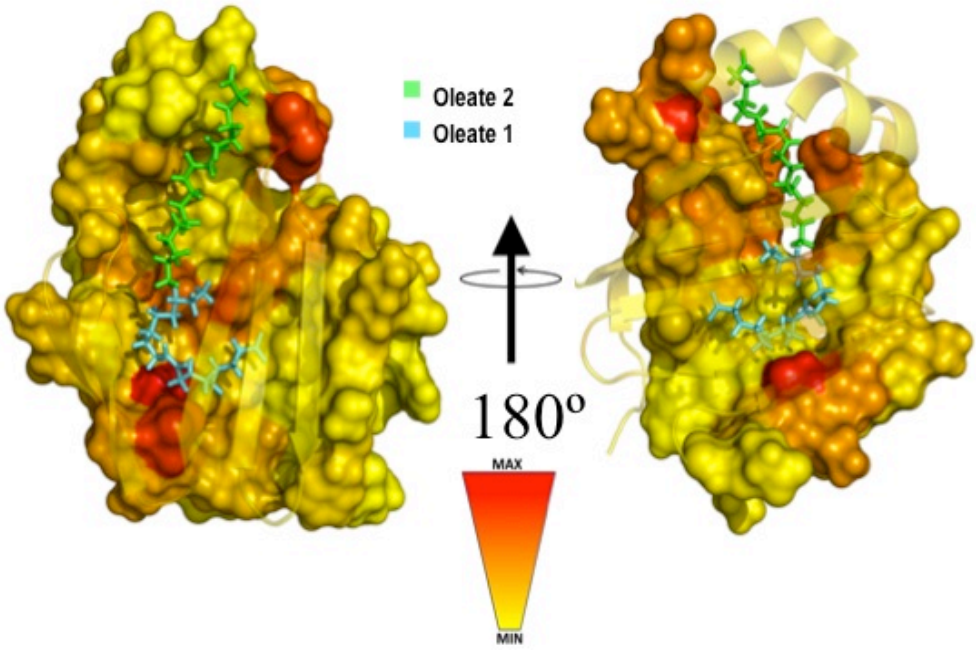

Figure 1.17. Difference in chemical shift between oleate- and linoleate-liganded LFABP mapped onto a three-dimensional structure shown in surface representation.
The color gradient from yellow to red shows gradually increasing differences observed in location of perturbation between the two ligands.

1.3.4.3. Exploring other LFABP ligands

a) Warfarin

Investigation of interaction of warfarin with LFABP by solution NMR was motivated by reported observations of Myszka and Swenson[18]. Oleate bound holo-LFABP was chosen as the starting point of our binding study considering two factors. First, literature evidence indicates comparison of oleate and warfarin binding, indicative of possible competition between the two ligands[18]. Second, considering the well-resolved HSQC spectrum of oleate liganded holo-

LFABP in folded state, it is rational to follow the interaction from the stable holo-LFABP. Initially, a large excess of warfarin was added to a complex of doubly liganded LFABP (molar ratio of protein:oleate is 1:2). Observing the chemical shift perturbation on the HSQC spectra superimposed in Figure 1.18, left panel, sequential titration points were recorded as described in Section 1.2.2.4.

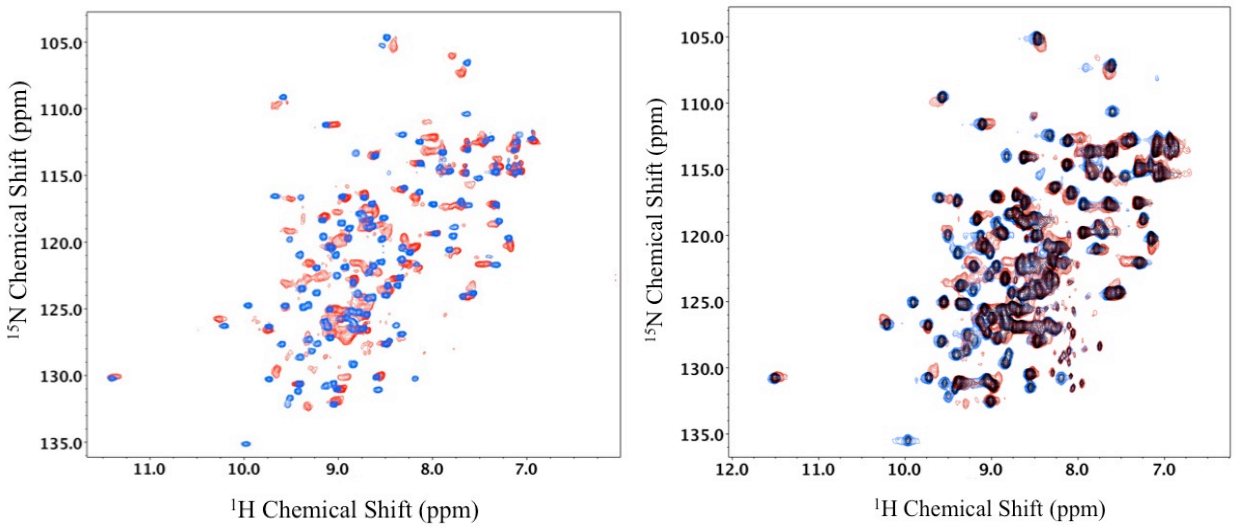

Figure 1.18. Overlaid HSQC spectra of doubly oleate liganded LFABP (blue) and added excess warfarin (red); right panel, spectra of left panel overlaid with spectrum in presence of 0.2eq warfarin (black).

Observing the HSQC spectra as presented in Figure 1.18, left panel, it is evident that holo-LFABP exhibits chemical shift perturbation upon addition of warfarin. In light of the peak broadening observed with sequential addition of warfarin, data were recorded only until 2 equivalents of added warfarin. HSQC spectrum in presence of 0.2 eq warfarin with oleate liganded LFABP is shown in Figure 1.18, right panel (black). In order to assign the backbone resonances in the presence of warfarin, three-dimensional experiments (TOCSY-HSQC and NOESY-HSQC) were recorded for holo-oleate-warfarin complex (large excess of warfarin was added to oleate liganded LFABP, where LFABP: oleate molar ratio was 1:2). However, only ~50% of the 127 residues were assigned due to poor spectral quality from the 3D experiments.

Owing to this incomplete assignment, the chemical shift perturbation could not be mapped on the sequence and the three-dimensional structure, since the incomplete resonance assignments would lead to misleading interpretations about the magnitude of chemical shift perturbation and location of binding.

b) Phytanic acid and Glucose

Phytanic acid was reported to bind to LFABP with K_d of 15 nM and 286 nM for the first and second ligand-binding site respectively measured by isothermal titration calorimetry[16]. In the case of phytanic acid, an excess of an isomeric mixture in 5 mM NaOH was added to the apo form of LFABP. Comparing HSQC spectra showed no evidence of chemical shift perturbation in presence of phytanic acid. In spite of claims that glucose binds to LFABP with a K_d of 103 nM in at pH 7.4, 24°C[17], chemical shift perturbation was not observed at the tested conditions of pH 7.0, 10°C. To be consistent with experimental conditions of oleate and linoleate interaction, test with glucose was performed using aforementioned conditions.

1.3.4.4. Conclusion

Observations of the binding characteristics of LFABP with several diverse ligands show some positive results, suggesting a path towards future explorations. To understand individual ligand binding to the protein alone, obtaining consistent and well-resolved HSQC spectra of apo-LFABP are of utmost importance. A possible reason for the poor spectral quality of the apo HSQC spectrum during this project can be lack of proper folding in absence of ligand. Comparison of oleate and linoleate binding shows a larger area of differential perturbation in the second binding site. Possibly an extra unsaturation confers different conformation of linoleate in the first site and thus requires greater area of interaction in the second site.

A result from preliminary trial with warfarin is encouraging. However, in order to confirm the location of probable competition of warfarin and oleate, complete backbone resonance assignments are required for the warfarin-oleate-LFABP complex. Further, the thermodynamics of this competitive binding can be investigated with isothermal titration calorimetry. Knowledge of molecular details of LFABP-warfarin interaction can shed light into the mechanism of action of warfarin as an anticoagulant drug.

Phytanic acid did not show chemical shift perturbation with LFABP; this might be attributable to the poor solubility of phytanic acid. In this regard, different experimental conditions should be tested. To validate, glucose as a potential ligand for LFABP, starting with oleate liganded holo-LFABP seems rational since glucose binding was reported to modulate affinity of LFABP towards lipid ligands[17]. However, considering the size and solubility of glucose, it is unlikely that it would go into the cavity of LFABP.

Chapter 2. Pedagogical Applications of LFABP Purification and Biophysical Visualization

2.1. Rationale for the Redesign of the CCNY Biochemistry Laboratory course

A biochemistry laboratory course is an essential component of any advanced level undergraduate biochemistry curriculum. Numerous drawbacks and opportunities for improvement were identified for the existing schedule of student experiments in the biochemistry laboratory course at the City College of New York. The main goal of this course is to expose students to basic biochemical techniques, complementing the concurrent lecture course by providing insight into how biochemical principles are established experimentally. In light of the need to revamp the current curriculum, a plan was made to incorporate a "research-inspired module", encompassing production, purification and biophysical characterization of liver fatty acid-binding protein (LFABP). The availability of a standardized protocol for production of LFABP in high yield (30 mg of protein per liter of bacterial culture) and well-defined structural biology, in terms of oleate-liganded solution-state nuclear magnetic resonance spectroscopic (NMR) and X-ray crystallographic structures[7,8], make LFABP a suitable candidate for biomolecular visualization. A three-session protocol was adapted from ongoing research activities to accommodate the 4-hour laboratory sessions run at CCNY. The rationale was to keep the basic lessons of amino acid titration, size exclusion chromatography and build on them by introducing an advanced "research-inspired" module. Incorporation of production, purification and characterization of LFABP was designed to enable students to follow a logically flowing story and to provide them

with a flavor of a basic research protocol within the confines of a laboratory exercise. Finally, the addition of an in-silico exercise provided a new modern component for the CCNY course.

2.2. Curriculum Plan: Critical Comparison of Existing and Proposed Designs

The existing curriculum (Table 2.1) has several deficiencies. First, it includes very old techniques, which are no longer practiced in traditional biochemistry laboratory research. For example, paper chromatography is an obsolete technique to analyze eluted fractions from column chromatography. Therefore, this technique may be replaced with UV/Vis analysis of fractions followed by ion-exchange chromatography as required, and the new curriculum will include modern in-silico investigation of protein molecular structure using the PyMOL software[25]. Second, the organization of the existing syllabus is redundant. For instance, the existing course (Table 2.1) begins with "protein assay" (session 1) but repeats this same experiment in session 6. Hence, session 1 may be omitted to create another "usable session" to introduce new biochemical methodology. Third, current labs 7, 8 and 11, 12 have each been completed easily in one session, generating two additional "usable sessions". Thus, a total of four "usable sessions" are available to incorporate a complete research-oriented laboratory module within the confines of an instructional laboratory course.

Considering the limited time available for protein production, the instructor will use session 5 to introduce the theory of transformation, protein overexpression by induction, and cell harvesting. Then, in session 6, students will carry out cell lysis (on a cell pellet provided by the instructor), and the supernatant will be loaded onto a manually packed size exclusion column or ion exchange column. Different student group will perform one chromatographic technique to compare the results. The degree of purification achieved by size exclusion chromatography or ion exchange chromatography will be analyzed by performing SDS-PAGE. In session 7, an *in-*

silico exercise will be performed using the NMR structure of oleate-bound LFABP as a model. During session 9 (after running SDS-PAGE in lesson 8), students will discuss their results from sessions 5-8.

The purpose of the new *in-silico* session is detailed visualization of the molecular structure of LFABP, which will enable the students to appreciate essential structure-function relationships. The freely available molecular visualization software package PyMOL will be used for this purpose. The instructor will guide students to visualize three-dimensional structures of proteins (e.g., LFABP) and small molecules (e.g., fatty acids), search for active sites, analyze the ligand-binding cavity, infer protein-ligand interactions, compare conformations of an apo-protein (without the ligand) and holo-protein (with the ligand), and generate multiple sequence alignments among FABP isoforms from different tissues and different species. The 4-hour duration of this exercise will allow the students to study LFABP structure in depth using PyMOL.

In the newly organized laboratory course (Table 2.2), the students start with the basic exercise entitled "Titration of an amino acid." This preliminary session introduces the chemical nature of amino acids. In the following session, the students apply the acquired knowledge (in "proposed" lab 2) to observe the behavior of amino acids in an electric field. The next two lessons (proposed lessons 3 & 4) are identical to existing sessions 5 & 6, in which students learn the important concepts of gel filtration chromatography, enzyme activity and protein quantification by the Bradford method. To introduce bacterial production of engineered proteins, reinforce the gel filtration exercise and add an in-silico molecular visualization component, the subsequent three sessions (Table 2.2) will comprise a research-based module focusing on LFABP. By designing

laboratory sessions with LFABP as the central theme, the research target of this dissertation can gain additional pedagogical and scientific impact.

The new course design is pedagogically significant because students will be exposed to the hierarchical organization of research biochemistry. The strength of this design also derives from the fact that it exposes the students to a range of logically related activities, spanning the basic rationale of production and purification of a recombinant protein and applications including molecular-level visualization and understanding of "their protein of interest" (in this case LFABP) during an *in-silico* exercise (proposed laboratory session 7). This module will give the students a global view of laboratory research encompassing protein production, purification, molecular conformation, and ligand recognition. It will enable students to understand and analytically evaluate the necessity of applying a biochemical technique. For example, the necessity of a second purification step can be evaluated critically by analyzing SDS-PAGE results after the first purification step (size exclusion chromatography, to be discussed in detail in Section 2.4.2.1). Additionally, the new design entails an opportunity to discuss a traditional research plan in lucid fashion to stimulate biochemistry students.

Simultaneously, the new design is scientifically significant; the designer faces the challenge of adapting a standard research protocol to fit within a shorter timescale. In addition, the designer must consider whether a protein preparation deemed pure in a student exercise meets research standards of purity.

In a nutshell, implementation of the proposed plan should be advantageous for the students. Moreover, the proposed design offers a more organized sampling of the principal steps of traditional biochemical research using the protein LFABP. Therefore, the proposed organization achieves improvements with respect to the existing course content.

	Title	Comments
Lab 1	Protein Assay	Repeated in lab 6.
Lab 2	Titration of an amino acid	
Lab 3	Separation of amino acids by paper electrophoresis	
Lab 4	Separation of Amino acids by ion-exchange chromatography and analysis by paper chromatography	Outdated, time-consuming method.
Lab 5	Purification of an enzyme: β-galactosidase (part 1: Size-Exclusion Chromatography)	
Lab 6	Purification of an enzyme: β-galactosidase (part 2: Protein Assay)	
Lab 7	Analysis of proteins by SDS-PAGE	Can be done in 1 session
Lab 8	UV-Vis Spectrophotometry of proteins	
Lab 9	Determination of Catalase activity	
Lab 10	Biological catalysis and oxidation-reduction using Lactate Dehydrogenase	
Lab 11	Small scale plasmid DNA isolation	Can be done in 1 session
Lab 12	Restriction enzyme digestion of plasmid DNA and polymerase chain reaction (PCR)	
Lab 13	Agarose gel electrophoresis	

Table 2.1. Existing Syllabus for Biochemistry Laboratory Course.

	Title	Lab number in existing Syllabus
Lab 1	Titration of an amino acid	2
Lab 2	Separation of amino acids by paper electrophoresis	3
Lab 3	Purification of an enzyme: β-galactosidase (part 1: Size-Exclusion Chromatography)	5
Lab 4	Purification of an enzyme: β-galactosidase (part 2: Protein Assay)	6
Labs 5-7	Lab 5: Introducing Liver fatty acid binding protein, descriptions of transformation of competent cells with the plasmid (containing LFABP gene), cell growth. Students will inoculate bacterial cell into petri-dish Lab 6: Cell lysis followed by gel filtration or ion exchange chromatography to purify LFABP (Different student groups will perform different chromatographic techniques and compare the results) Lab 7: *In-silico* exercise using NMR structure of oleate bound LFABP as a model	New sessions
Lab 8	UV-Vis Spectrophotometry of Cytochrome-C and SDS-Polyacrylamide gel electrophoresis of saved samples from LFABP purification (lab 6)	No change
Lab 9	Discussion of results from sessions 5-7 followed by analysis of SDS-PAGE performed in session 8	
Lab 10	Biological catalysis and oxidation-reduction using Lactate Dehydrogenase	
Lab 11 & 12	Small scale plasmid DNA isolation, Restriction enzyme digestion of plasmid DNA and polymerase chain reaction (PCR)	
Lab 13	Agarose gel electrophoresis	

Table 2.2. Proposed Syllabus for Biochemistry Laboratory Course.

In the following section a student handout is presented for the proposed "research-inspired" laboratory sessions (5-7). Specific notes to the instructor are embedded in the students' handout as necessary. Followed by the handout, results from a preliminary trial performed with undergraduate students are presented.

2.3. Lab Session 5: Introduction to LFABP

2.3.1. Fats & Fatty acids

Lipids are one of the most important constituents of animal and plant cells. They are a chemically diverse group of compounds classified together because of their apolar structures, which give them very low solubility in the aqueous environment of the cell. This low solubility equips lipids for one of their most important functions, which is to serve as the major structural elements of the biological membranes that surround cells and partition them into various compartments. Unlike other biomolecules (proteins, nucleic acids, and polysaccharides), lipids are not polymers; instead they are comparatively smaller with structures such as that shown in Figure 2.1. Owing to their structural features, lipids tend to assemble together in an aqueous environment. The force driving such association is non-covalent in nature and stems from two fundamental sources: i) non-polar tails of lipids associate via an entropy-driven hydrophobic effect; ii) the van der Waals interaction between the hydrocarbon regions of the molecules is energetically favorable. The polar, hydrophilic head groups of the lipid molecules, on the contrary, tend to associate with water. Thus lipids are actually "amphipathic" by nature. [Modified from[26]].

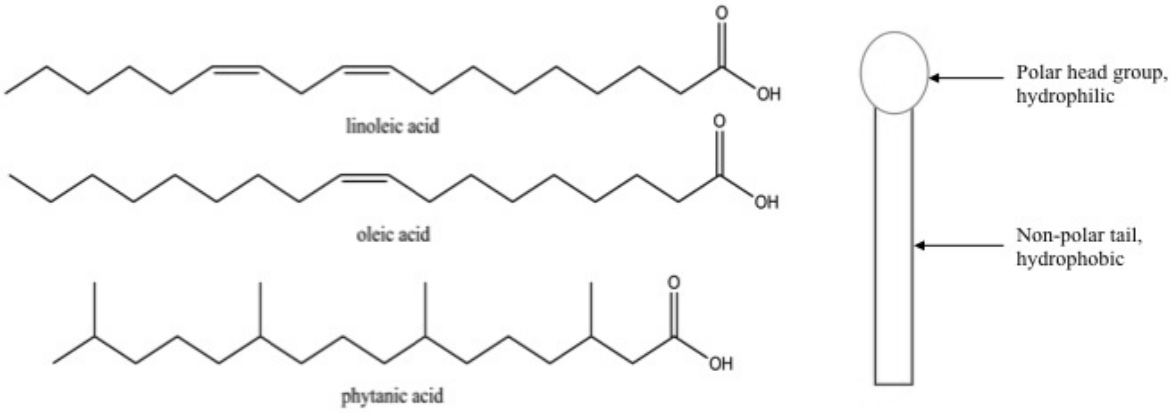

Figure 2.1. Structures of Fatty acids.

Apart from serving as major constituents of biological membranes, lipids also function in energy storage.

The simplest of lipids are the fatty acids, which are also constituents of many more complex lipids. Fatty acids are building blocks of phospholipids, which are major constituents of biological membranes. Vitamin esters also contain fatty acids. Fatty acids function in energy storage in the form of triacylglycerols. The chemical structure of fatty acids conforms to the general lipid structure (shown in Figure 2.1). Fatty acids are either saturated (having single bonds only) or unsaturated (with one or more double bonds). Many important naturally occurring fatty acids are unsaturated with one or more double bonds. Oleic acid (shown in Figure 2.1), which is found in many animal fats, has one double bond (therefore it is monounsaturated) between carbons 9 & 10 from the carboxyl end of the molecule. In terms of chain length, oleic acid, with 18 carbons, is categorized to be a long-chain fatty acid or LCFA.

2.3.2. LFABP

LCFAs often require a carrier, owing to their hydrophobic non-polar tail, to reach different organelles inside the aqueous cellular environment. For this purpose there exist special classes of proteins, which are the intracellular lipid binding proteins (iLBPs)[27]. Intracellular lipid binding

proteins comprise nine mammalian fatty acid binding proteins (FABPs) from different tissues, cellular retinoic acid binding proteins and cellular retinol binding proteins. The FABPs are abundant cytosolic, ~15-kDa proteins that comprise 5% of the total protein in the cytosol. Among these, liver fatty acid binding protein (LFABP) is unique within the intracellular lipid binding protein family because of its ability to bind more than one molecule of long-chain fatty acid simultaneously and to bind other diverse ligands with high affinity[8](Figure 2.2). It is noteworthy that one of the oleate molecules actually binds to a region of the protein within a well-defined cavity. Structural investigation of LFABP indicates that the interior of the cavity is composed of non-polar hydrophobic residues. The three-dimensional tertiary structure of LFABPs is highly conserved among different species, including 10 anti-parallel β-strands forming a β-barrel capped by a helix-turn-helix loop. LFABP has 127 amino acid residues in its primary sequence, and it exhibits 22%-73% sequence homology to FABPs from other mammalian tissues.

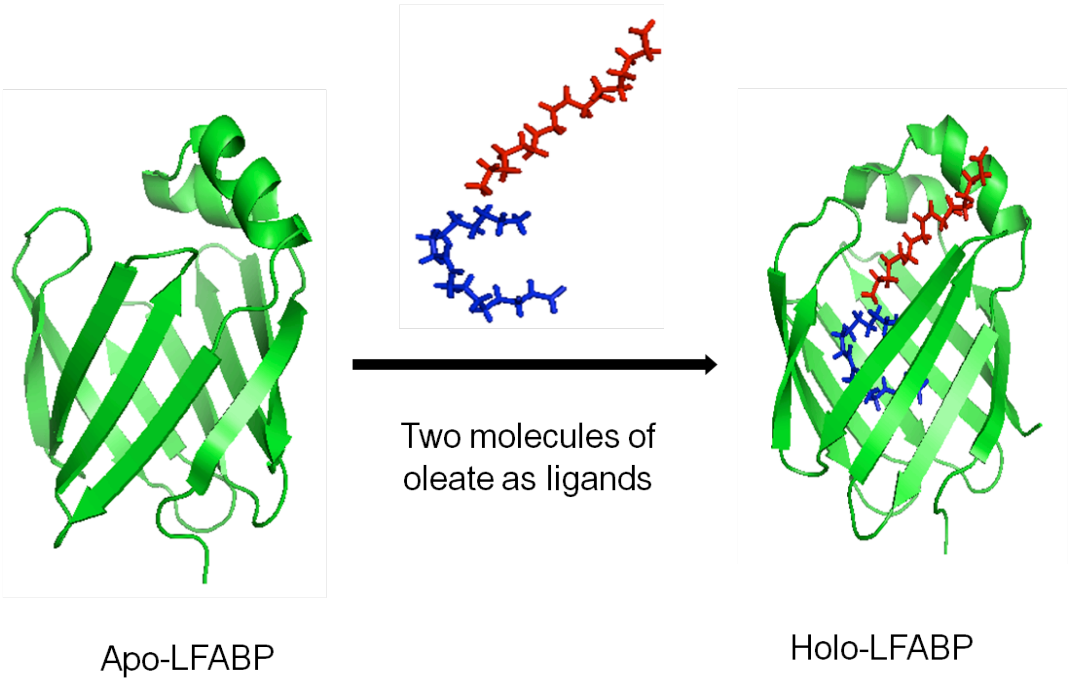

Figure 2.2. Solution state NMR structure of Liver fatty acid binding protein bound to oleate.

For the production, purification and characterization of LFABP a general scheme is represented below:

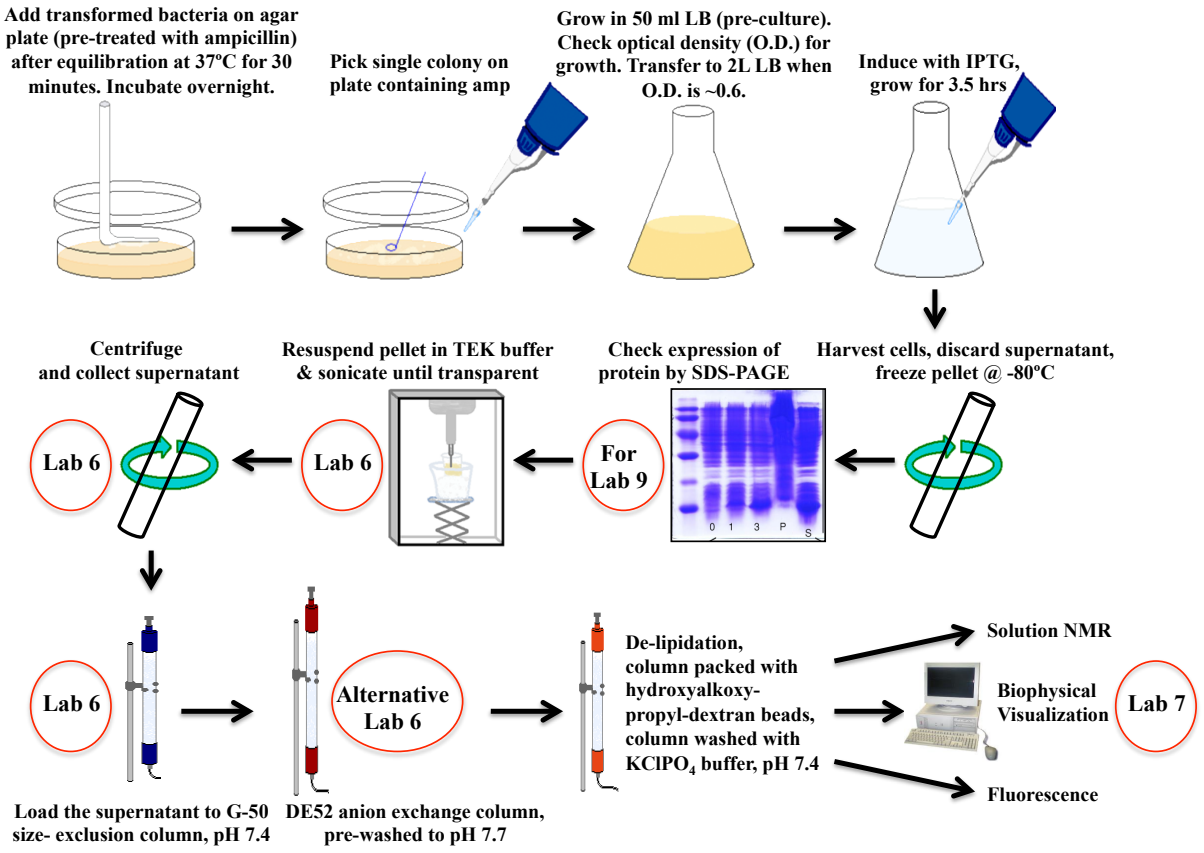

Figure 2.3. A schematic overview of production and purification of LFABP.

2.3.3. Pre-lab questions

As a prelude to the lab session 5, students should be guided to answer the following pre-lab questions:

1. What do you know about fatty acids? Illustrate your idea about their molecular structure, chemical properties, and biological functions.

2. Jane inadvertently introduced a strand of hair in the petri dish during inoculation. Is it going to affect the experiment? If so, describe an appropriate way to handle the situation.

3. From gene of your interest, how do you produce protein?

2.4. Lab session 6: Production of LFABP

2.4.1. Note to the instructor

An expression vector is a modified plasmid (plasmids are extra-chromosomal, self-replicating, double stranded circular DNA). Expression vectors are generally plasmids containing resistance to an antibiotic that transport a gene into an appropriate host cell (often E. coli) and direct the synthesis of the encoded protein product. In order to direct specific protein synthesis, expression vectors must also contain the regulatory elements for initiating transcription of the gene encoding the protein and subsequent translation of the produced mRNA.

Yield is an important parameter to achieve large-scale production of a protein. In this regard, the instructor should discuss the importance of fresh transformation of the recombinant expression vector into competent cells. Transformation refers to the uptake of foreign DNA (which is often recombinant plasmid DNA containing the gene of interest) by a suitable host cell, often E. coli. This organism is used widely for cloning purposes in recombinant DNA research, because it has a reasonable generation time of about 20 minutes and is cost-effective. However, E. coli is not naturally competent to take up foreign DNA from the surrounding medium. Competence can be conferred upon E. coli by artificial means, for example by heat shock or by electroporation. The state of competence is actually a transient physiological state of E. coli particular to the exponential growth phase and influenced positively by calcium ions. We will use commercially available competent BL21 (DE3) cells to introduce the gene encoding LFABP in the form of an expression vector. The transformation protocol follows:

1. *Thaw competent cells on ice. Gently mix cells. Do not mix cells by pipetting.*

2. For transformation of BL21(DE3) competent cells with recombinant plasmids containing the gene of interest, add 5-10 µl of the plasmid DNA (0.2 to 50 ng DNA) to the cells.

3. Incubate cells on ice for 30 minutes.

4. Heat-shock cells for 40 seconds in a 42ºC water bath; do not shake.

5. Place on ice for 2 minutes.

6. Add 0.9 ml room temperature SOC medium (Super Optimized broth with Catabolite repression).

7. Shake at 225 rpm (37 ºC) for 1 hour.

8. Spread 100 µl of transformed cells on LB agar plates containing 100 µg/ml of the antibiotic ampicillin.

9. Incubate overnight at 37 ºC.

Performing the transformation protocol might not be practical, since competent cells are expensive. The instructor should discuss the principles of transformation, bacterial growth curve and principles of sonication.

Students may be divided into two groups to perform size exclusion chromatography or ion exchange chromatography on the cell lysate. This procedure would provide an opportunity to compare the usefulness of two different chromatographic techniques. The complete protocol represented here has been adapted from research activities in the Stark lab; the protocol was originally devised by Ockner et al[1] and later modified and revised by the Storch group[13] and the Stark group[8].

2.4.2. Production of LFABP

To produce rat LFABP, we start from the gene encoding the rat LFABP protein. We have the L-FABP gene in the form of recombinant DNA expressed in a pET11a expression vector. Cell lysis

is followed by size exclusion chromatography using gravity columns. Gel filtration columns, which separate proteins according to their size, are packed with tiny, porous Sephadex G-50 beads. Molecules that are small enough to enter the pores stay inside the beads as they travel down the column, while larger molecules remain in solution by flowing between the beads and therefore emerge more swiftly from the column. Besides providing a means of separating molecules based on their sizes, gel filtration chromatography is a convenient way to estimate their size.

2.4.2.1. Protocol for Cell lysis & gel filtration chromatography

1. The instructor will provide cell pellets (frozen at the end of induction by isopropyl thio-galactoside (IPTG) and then harvested) to each student group.
2. Thaw the cell pellets, add 7ml of TEK lysis buffer (10 mM Tris, 1mM EDTA, 100 mM KCl, pH=8.3 at 4ºC).
3. Add 7µl of 100 mM stock PMSF solution (protease inhibitor) to a final concentration of 0.1µM.
4. Lyse the cells using pulse mode sonication (sonicator equipped with a micro-tip) at a power level of 5 (0.5 sec pulse on, 1 sec pulse off); repeat 8-12 times. The solution should become semi-transparent.
5. Centrifuge for 45 minutes @ 19,000 rpm and 4ºC.
6. Save pellet (just enough on a tip of toothpick) and mix with 50 µl of 1X sample buffer for analysis by SDS-PAGE; retain the remaining pellet at -80 ºC.
7. Mix 50 µl supernatant with 50 µl of sample buffer for analysis by SDS-PAGE.
8. Load 400 µl supernatant onto a Sephadex G-50 size exclusion column that contains medium coarse beads packed manually under gravity to a column volume of 20 ml and pre-

equilibrated with 0.15 M KCl and 0.01 M phosphate buffer at pH 7. Performing the chromatography at room temperature does not alter the protein's biological activity.

9. Use a stopwatch to measure the flow rate of the column at 270 µl/min (ascertained by weighing an empty Eppendorf tube, collecting flow through from the column (per minute) in that tube, weighing the tube again, the difference gives the volume eluted from the column in one minute).

10. Collect 70 fractions (2min/ fraction).

11. Dilute 20 µl from each tube to 800 µl, and then record the absorbance of each dilute sample at 280 nm using an UV/Vis spectrophotometer.

12. Plot the data using EXCEL, showing UV absorbance on the y-axis and fraction number on the x-axis (a representative UV absorbance profile is shown in Figure 2.5, left panel).

13. Perform SDS-PAGE (during lab session 8) on selected fractions and analyze data to decide if further purification steps are necessary.

2.5. Lab Session 7: Exploring LFABP using PyMOL

2.5.1. Note to the Instructor

First, PyMOL[25] must be installed in the computer students are going to work with. The minimal system requirements for installing PyMOL are: i) Windows 98 and ME (millennium edition), ii) 3D Open GL compatible graphics accelerator card, iii) 256 MB RAM, iv) 500 MHz Pentium 3 processor. For more information, visit www.PyMOL.org. Upon clicking PyMOL icon, two simultaneous windows will appear; one is the PyMOL viewer, used to view the three-dimensional cartoon representation of the molecule of interest. At the top of the PyMOL viewer window there is a GUI window (which uses the Tcl/Tk scripting language) to view, manipulate and analyze molecules using a command line.

At the beginning of the session, the fundamentals of biomolecular structures (primary, secondary, tertiary and quaternary), molecular geometry and molecular interactions will be briefly reviewed. Utilizing PyMOL students will be able to visualize primary and secondary structures (α-helices and β-strands) of a protein. Similarly, the concepts of tertiary conformation and quaternary structure (as in hemoglobin tetramer) will be illustrated. At the outset the students will explore the web-based resource, PyMOL, which will then be used more extensively to examine LFABP. Finally, the students will be introduced to protein structures through the RCSB protein data bank (PDB). This database stores experimentally solved (by X-ray crystallography or nuclear magnetic resonance spectroscopy) three-dimensional structures of proteins, nucleic acids and macromolecular assemblies. After the initial overview, the students will appreciate that specific pdb codes are assigned to particular proteins for easy reference.

This brief overview will be followed by more complex tasks using PyMOL. For instance, the program is capable of showing or hiding different representations of a macromolecule. Thus LFABP may be observed either in line/stick/cartoon/ribbon/surface forms. This range of representation is especially effective to identify different secondary structural elements (α-helices, β-strands), to analyze the ligand-binding site, and to interpret protein-ligand interactions.

Students will be directed to perform the following exercises regarding the interaction of oleate with LFABP. Possible questions are presented at the end of the session. The objectives are as follows:

1. *Compare the conformations of apo and holo LFABP.*
2. *Identify key amino acid residues involved in binding oleates at two different sites. For example, residues R122, S124, K125, R126 among those involved in first ligand binding and*

G32, K33, D34, I35, G37 among those involved in second ligand binding [12] would be of interest. Discuss the chemical nature of those amino acid residues and therefore develop hypotheses regarding the driving force of LFABP-oleate interaction at those sites. Specifically highlight polarity and hydrophobicity of amino acid residues comprising the ligand-binding site.

3. Observe the specific orientations of the two oleates (oleate in the cavity has a "U" shaped conformation, whereas the oleate closer to the portal region of LFABP has an extended, conformation). Identify possible reasons for such conformational heterogeneity of the same molecule bound to the protein.

2.5.2. Visualizing the solution state NMR structure of rat LFABP

2.5.2.1. Protocol

The stepwise protocol for visualizing solution state NMR structure of rat LFABP is presented in the following list:

1. Click on PyMOL icon.
2. Go to file→open→2ju8.pdb (the pdb code 2ju8 designates the three dimensional structure of oleate liganded (in 1:2 protein:oleate ratio) LFABP solved by solution-state NMR[8].

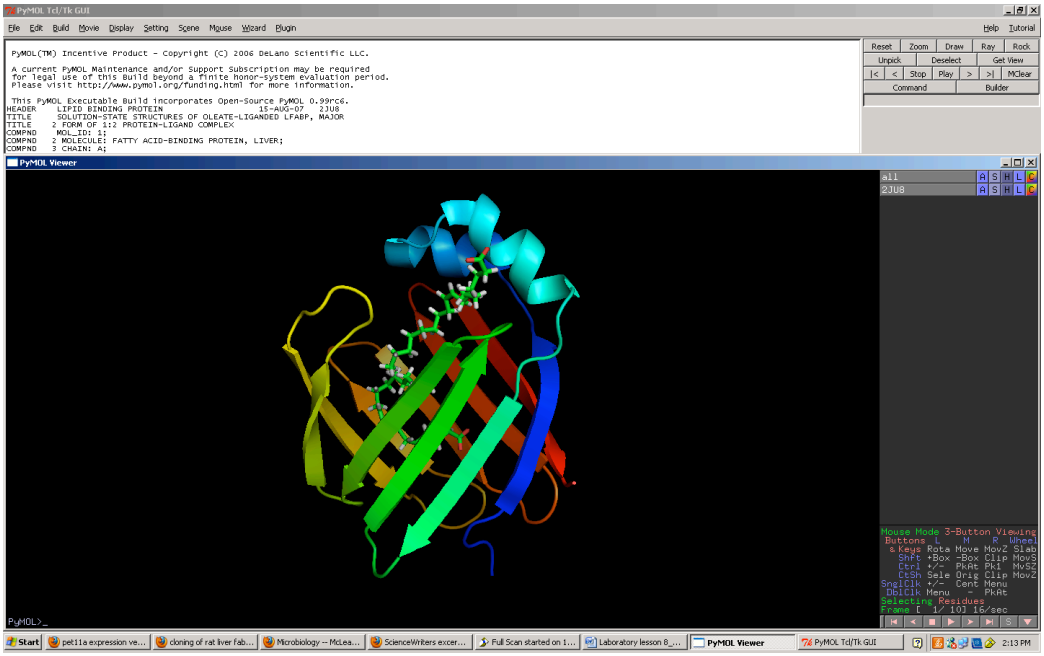

Figure 2.4. Screenshot of PyMOL session showing solution state NMR structure of LFABP bound to oleate.

3. Usually, the "line" representation of LFABP will show up at this stage.

4. As beginners, students should practice visualizing different representations. Students will observe LFABP on the PyMOL viewer window (as indicated in Figure 2.4). On the top, extreme right of the window the tab "2ju8" will show up when step 2 is performed.

5. Beside the tab "2ju8" there are the following tabs: A-all; S-show; H-hide; L-label; C-color (as discussed in 9-12) below.

6. Using the "show" tab, display line/ stick/ ribbon/ cartoon representation (s).

7. At the top of the window, go to "display→sequence on→this will display the amino acid sequence of LFABP.

8. Save your work. The importance of saving a session or an image cannot be emphasized too strongly. To achieve this task, go to file→save session or save as image. This ensures that work from one or more sessions is not lost and when returning you do not have to start from scratch.

9. The “show/hide” feature of PyMOL enables one to selectively observe (by choosing the “show” tab) specific regions of the protein while hiding others. This feature is especially important to observe and analyze the three-dimensional structure from different angles.

10. Bringing the cursor onto the sequence and clicking and dragging enables visualization of specific segments of the protein. For example, it is possible to selectively hide parts of the sequence to visualize other parts specifically; on the other hand, representation of various segments of LFABP in different formats (for example, cartoon vs surface) is also possible. This feature of PyMOL is especially useful for careful investigation of the oleate-binding site of LFABP. For efficient display and inspection of various parts of the protein in different representations, the command “cartoon transparency” is quite useful; this feature can create better visibility for overlapping regions of the surface.

11. Label the structure. It is relevant that, utilizing the “L-label” tab, it is possible to label the three-dimensional molecular structure of interest. This scheme can involve labeling as residues/ as residue name/ chain, etc. Here using the show/hide feature you can closely analyze individual amino acid residues after labeling them using the “residue name” option.

12. Color the structure. The tab “C-color” is very effective in selectively coloring different parts of the molecule differently. A sophisticated application of the coloring function is the “preset” tool under “all” tab. With any form of representation (line/stick/cartoon), clicking “preset” → “pretty with solvent” will color the protein according to its secondary structural elements. This sort of color-coding is useful in identifying secondary structural elements.

13. Structural analysis of LFABP

a) Investigation of the ligand-binding site of LFABP: Spatial investigation of the oleate-binding site is at least as important as sequence-specific investigation of the binding site. Since the spatial location of amino acid residues are governed by their chemical nature. As mentioned in step 9 above, by manipulating the selective display option (cartoon vs surface), different regions of LFABP (involved in ligand binding) can be viewed as cartoon or as surface representations. This procedure facilitates identification of residues at the ligand-binding site. Interesting residues would be R122, S124, K125, and R126 in the first ligand-binding site and G32, K33, D34, I35, G37 in the second ligand-binding site.

b) Investigation of the cavity of LFABP: Investigation of the holo-protein in the cartoon representation clearly indicates that LFABP possesses a cavity.

14. Analysis of LFABP-oleate interaction

a) Investigating by residue: This will shed light on the molecular mechanism of the interaction between oleate and LFABP. Understanding the chemical nature of the amino acids involved in oleate binding is imperative to understanding the forces stabilizing such an interaction. For example, polar residues will be mostly stabilized by electrostatic interactions and hydrogen bonds, whereas non-polar or hydrophobic residues will be stabilized by hydrophobic forces, which are entropy-driven. Using PyMOL it is possible to identify the key residues involved in interaction of oleate with LFABP. This will lead to understanding of the possible forces involved in stabilizing such interactions.

b) Forces involved in LFABP-oleate interaction: Knowledge about key residues at the ligand-binding site may indicate the preferred chemical state of an LFABP ligand. With this information, students should identify key resides at the ligand binding site. Next, they would

specify the chemical nature of those identified residues saying whether they are polar/non-polar and charged/uncharged (in case they are polar). The chemical nature of the amino acids will be indicative of the preferred ionic state of the fatty acid at the ligand-binding site. Hint: Lysine (Lys) is a key residue at the ligand-binding site of LFABP. This information will in turn identify principal chemical forces stabilizing the ligand-protein interaction.

c) Measuring intramolecular distances between different residues of the protein is an interesting exercise. This is done in PyMOL by clicking on wizard→measurement. In order to measure the distance, first two amino acids of the protein structure must be selected. Then, clicking the measurement tab will display the distance in angstrom units. Knowledge of distances will quantify the understanding of location of residues, which are not adjacent in the primary structure, thus consolidating step 14.a) above further. Measure distances between key residues (as identified in 13.a) with oleate ligand at the site of interaction.

d) Specific investigation of two oleates: It is interesting to observe and identify the conformations of the two oleates at their respective ligand-binding sites on LFABP. Note that, oleate in the cavity shows an U-shaped conformation, while oleate closer to the surface exhibits an extended conformation.

e) Once again, saving the work is extremely important. This can be done by either saving the PyMOL session (click the "save session" tab on the top left hand corner) or clicking the file menu→save session option.

15. Comparing the NMR structure of LFABP with closely related proteins

It is intriguing that LFABP is co-expressed in the intestine as well as the liver. From the literature we also know that intestinal fatty acid binding protein (IFABP) belongs to the same family of intracellular lipid binding proteins (iLBPs, as mentioned in session 5) as LFABP.

Moreover, despite having the same tissue-specific origin and apparent structural similarity, IFABP binds only one equivalent of oleate in comparison to two equivalents of oleate bound by LFABP. Therefore, it would be an interesting in-silico exercise to compare the different ligand binding characteristics of IFABP vs LFABP. It is possible to compare NMR or crystal structures of recombinant rat LFABP with structures of closely related proteins. For example, it may be interesting to look at the crystal structure of human LFABP, NMR structure of intestinal fatty acid binding protein[10] (IFABP) (apo protein: 1AEL[10]; palmitate-bound[28]: 1URE (solution state NMR structure); crystal structures with bound myristate[29] and oleate[29] (bound with a point mutation), 1ICM. Calculating Root Mean Square Deviation (RMSD), using the "align" command in PyMOL, will be useful in comparing and understanding diversity of these protein structures.

2.5.2.2. Sample questions for lab session 7

The specific questions to be addressed using PyMOL are as follows:

a) Describe primary, secondary and tertiary structures of a protein.

b) What are the structural features of the cavity? Is it mainly β-sheet? What do you think about the role of α-helices in forming this cavity?

c) Following the color-coding exercise, investigate and record the number of β-sheet and α-helix elements. What kinds of chemical bonding are involved in stabilizing these structures?

d) Why the cavity is designed the way it is. What is its amino acid composition? Do we observe a specific class of amino acids lining the interior of the cavity? If so, what is the rationale behind such observations? How do we interpret the interaction of oleate in light of such observations?

e) What is the visual appearance of the oleate located inside the cavity as compared to the oleate closer to the (polar) surface of LFABP?

f) In terms of ligand binding (oleate with LFABP vs. palmitate with IFABP) do you see any differences between IFABP vs LFABP? How is the binding site situated -- in a cavity or towards the surface?

g) Propose a rationale for the specific ligand binding characteristics of IFABP as compared to LFABP.

h) Can you identify specific regions on the protein (a helix, loop, etc.), which have a distinct conformation in the holo (ligand-bound state) as opposed to the apo (protein alone state)? What does this observation suggest about structure-activity relationships in IFABP?

i) Do you think mutating the protein into a helix-less variant would alter ligand binding? Come up with a rationale. (Hint: consult the pdb using the key word "intestinal fatty acid binding protein").

j) What are the structural differences between solution NMR structures of the helix-less variant of IFABP (pdb code: 1A57) bound to palmitate with the wild-type IFABP (pdb code: 1URE) bound to palmitate? (Hint: look for residues close to the ligand in the wild-type IFABP and compare with the helix-less variant).

k) Come up with a rationale for the role of one or both helices in the interaction of IFABP and oleate.

2.6. Results from preliminary trial of lab sessions 6 & 7

The proposed laboratory sessions 6 & 7 were performed with undergraduate students in our research lab. In spite of initial challenges, the results were quite encouraging. Figure 2.5, left panel shows the 280 nm UV absorption profile of eluted fractions from a manually packed gel

filtration column (bed volume of 20 ml). It is worth noting that the protein of interest is present mainly in pure form apart from some minor impurities. However, it is noteworthy that the UV-absorption profile of gel filtration fractions and subsequent SDS-PAGE of the traditional research protocol (Figure 2.5, right panel) differs significantly from the observed result in this trial (Figure 2.5, left panel). In the traditional research protocol (Figure 2.5, right panel) the protein is only partially pure in most of the fractions, compared to almost pure protein obtained during the trial. That discrepancy might be attributed to the differences in column volume, mode of flow (gravity flow) and flow rate in the trial compared to the traditional research protocol. It should be noted that yield of purification was not as important for instructional purposes as for research protocol.

During the initial set-up, manual operation of the gravity column was challenging. There were some mistakes in fraction collection while monitoring the process manually. These were improved with repeated trials.

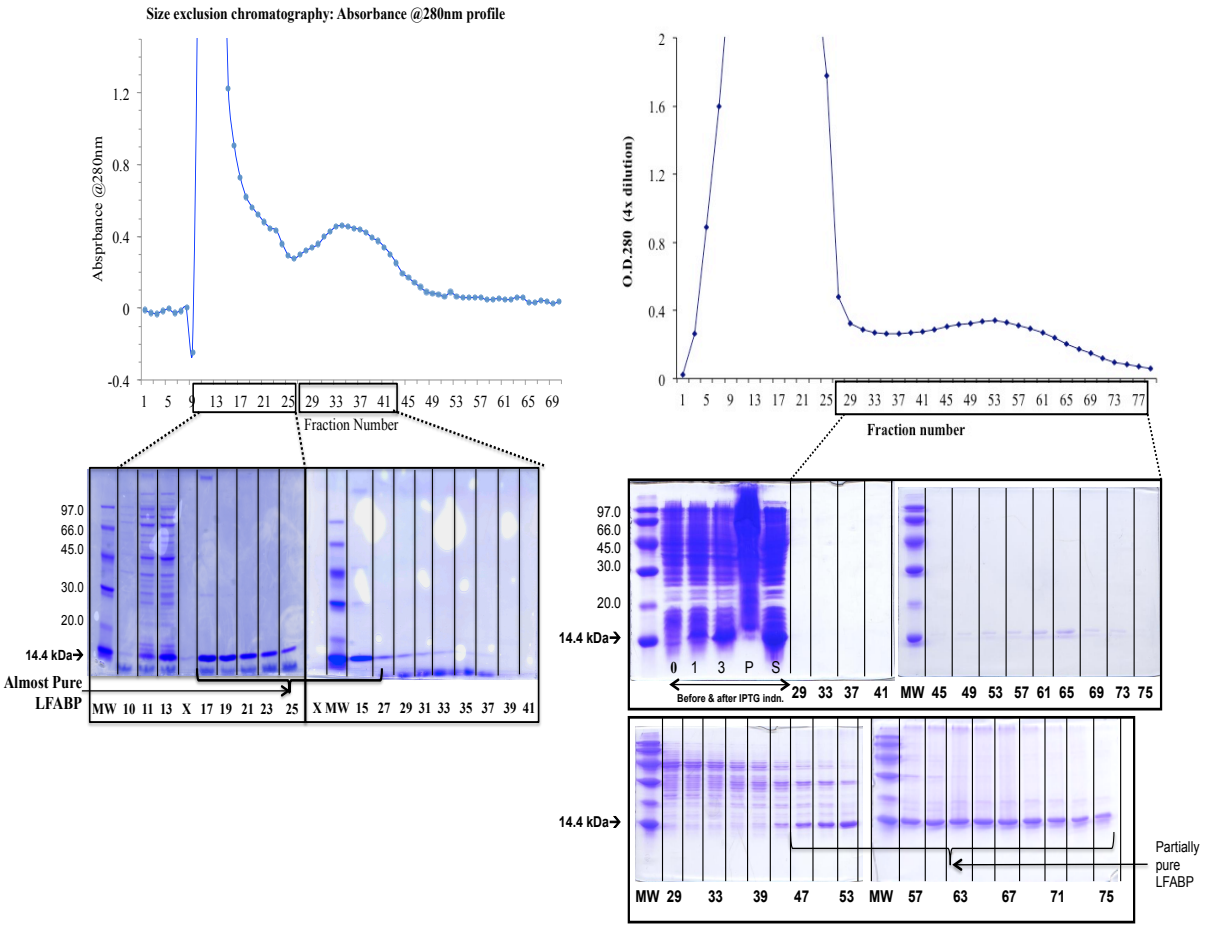

Figure 2.5. Comparative analysis of gel filtration elution between research and students' trial. Left panel: Students' trial, right panel: research protocol.

PyMOL exercise (lab session 7) was also tried with students at different levels from beginning graduate student to high school students. A screenshot of this trial session is presented in Figure 2.6. Students' response was enthusiastic despite initial confusions regarding various functionalities of PyMOL viewer, for example 'show', 'color', and distance measurements.

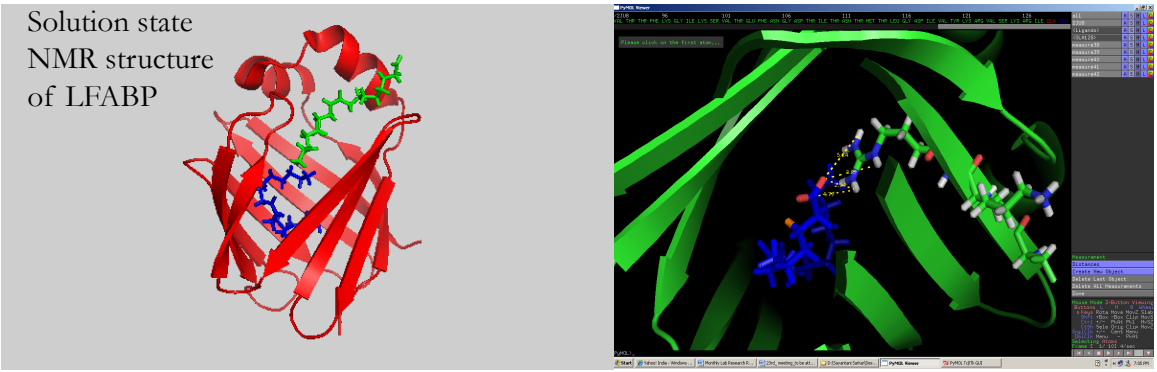

Figure 2.6. Screenshot of student PyMOL session.

Importantly, the sessions were implemented using basic equipment and supplies considering practical feasibility. Usage of manually packed gravity columns testifies this fact. This ensured that set-up was cost effective. Also, it is worth noting that the trial of sessions 6 & 7 could be completed within the stipulated time of 4 hours for each session. Specifically, cell lysis and gel filtration chromatography procedure was completed in 2.5 hours, keeping enough time for preparatory set-up prior to the experiment and discussion at the end.

From this student trial, important feedback was obtained, which will be useful for future implementation. For example, during the purification, ultracentrifugation helped students learn the principles of separation of cellular constituents based on their size correlated with centrifugation speed. Also, running the size exclusion column manually helped in understanding technical details of the chromatographic process. Additionally, performing SDS-PAGE provided the ability to learn and analyze results of purification. For students, the PyMOL session provided a novel approach to visualize the protein of interest at the molecular level to correlate structure and function. In sum, the proposed design was able to provide flavor of basic research to the students.

Chapter 3. Touring the Tomato: A Suite of Chemistry Laboratory Experiments

(A draft manuscript for the Journal of Chemical Education)

3.1. Introduction

The tomato fruit is a familiar ingredient of our everyday meals, yet its importance transcends nutrition to also include bioengineering and agriculture. Chemically, a tomato fruit contains a wide variety of biopolymers such as polysaccharides, waxes (lipids) and cutin (biopolyester). These biopolymers are accessible at molecular level by common analytical techniques. Starting from a simple analysis of mass percent of water, an intricate molecular picture can emerge by employing several analytical tools. Thus, the tomato fruit can function as a readily available storehouse of unique biopolymers capable of serving as a model for teaching several complementary analytical techniques at the same time.

This article describes development of laboratory course modules based on a panel of experimental techniques, UV-Vis spectroscopy, high performance liquid chromatography (HPLC), nuclear magnetic resonance (NMR) spectroscopy and atomic force microscopy (AFM) to probe various constituents of the tomato fruit. This course design is also appropriate for implementing the illustrated experimental techniques to address composition and properties of a wide range of biological macromolecules and assemblies. As an illustrative example, the lessons learned with tomato can be applied to grapefruit, carrot, and beet among fruits/vegetables, to textile, plastic helping to understand their constituent biopolymers at the molecular level.

3.2. Justification

The experience of applying analytical tools to investigate biopolymers can build the foundation for an interdisciplinary training encompassing common areas of biology and chemistry. Taking into consideration published *J. Chem. Ed.* articles related to tomato juice and the lycopene pigment[30-32] and other relevant work, we have designed a comprehensive set of modules adaptable for undergraduate as well as high school students. This laboratory curriculum derives from biophysical research on the tomato fruit[33]. This unique laboratory course aims to teach a battery of analytical techniques based on an inexpensive but comprehensive source of a wide range of biomaterials.

For high school students, the first five sessions (as shown in Table 3.1) constitute a short, yet comprehensive suite of experiments comprising applications of several analytical techniques studying macroscopic aspects, such as water percent, thickness and pigment characteristics of tomato cuticle. Following these modules, microscopic investigations of cuticular constituents by NMR and AFM pave the way for a molecular "tour" into the tomato fruit. Modules 6-8 may be demonstrated for high school students depending on available equipment. Alternatively, modules 6-8 can be organized as "mini project" to several groups of students. Students can transfer the experimental skills learned from the modules and develop their own projects. Therefore, these "mini projects" can include independent ideas from students about commonly encountered biopolymers in fruits/vegetables and suitable experimental design to investigate such biopolymers.

In case of students at undergraduate colleges or research institutions, the complete module can be laid out in 8 sessions with an approximate duration of 2-3 hours each. The order of presentation of the modules is flexible depending on learning objectives of different curricula and logistical

considerations. If for instance, a solid-state NMR facility is not available, similar information about functional groups of dewaxed tomato cuticle can be obtained from (Fourier transform) infrared spectroscopy. Details of this alternative procedure are discussed in the supplemental information.

Module	Experiment[a]	Discipline[b]
1.	Mass percent of water in tomato	G, A
2.	Thickness of tomato cuticle	A, BP
3.	Enzymatic removal of cell walls from tomato cuticle	BC
4.	Lycopene characterization by UV/Vis absorption spectroscopy and HPLC	A, BC
5.	Dewaxing of fruit cuticles by chloroform extraction	A, O
6.	*Structural fingerprint of cuticular waxes by solution-state NMR*	*BP*
7.	*Surface analysis of tomato cuticle by AFM*	*A, O*
8.	*Molecular profile of dewaxed cuticle (cutin) by solid state NMR*	*BP*

Table 3.1. Summary of Laboratory Modules.
[a]Optional modules are noted in italics, [b]Disciplines are General, Analytical, Biophysics, Biochemistry and Organic Chemistry. Each experiment has an approximate duration of 2-3 hours.

In sum, this design aims to "tour" the tomato, starting with mass percent of water, reason for coloration, and cuticle thickness, followed by delving deep into the molecular architecture by NMR and AFM. Therefore, this design illustrates that using a common subject, such as tomato as the central theme, several complementary analytical techniques can be taught.

3.3. Instruments

To conduct this panel of biophysical/analytical experiments, a chemistry laboratory is expected to be equipped with an analytical balance, drying oven, incubator-shaker, UV-Vis

spectrophotometer and high-performance liquid chromatograph (HPLC). An NMR spectrometer (details included in the supplemental document) and an atomic force microscope are also required. Note that, solid state NMR and AFM can be restricted to demonstrations only and "mini projects" involving investigation of biopolymers in common fruits/vegetables, can be included during the time allocated for these sessions. The goal is to have the students design their own projects as an outgrowth of the structured experimental module offered.

3.4. Experiments

An overall scheme summarizing the experimental modules is presented in Figure 3.1. The module starts with measuring the mass percentage of water, one of the main constituents of tomato fruit. Following studies on mass percent of water, thickness of tomato cuticle, characteristics of lycopene pigment are studied; afterwards the structural signature and surface characteristics of tomato cuticle are investigated by NMR and AFM, respectively providing a molecular view of the fruit.

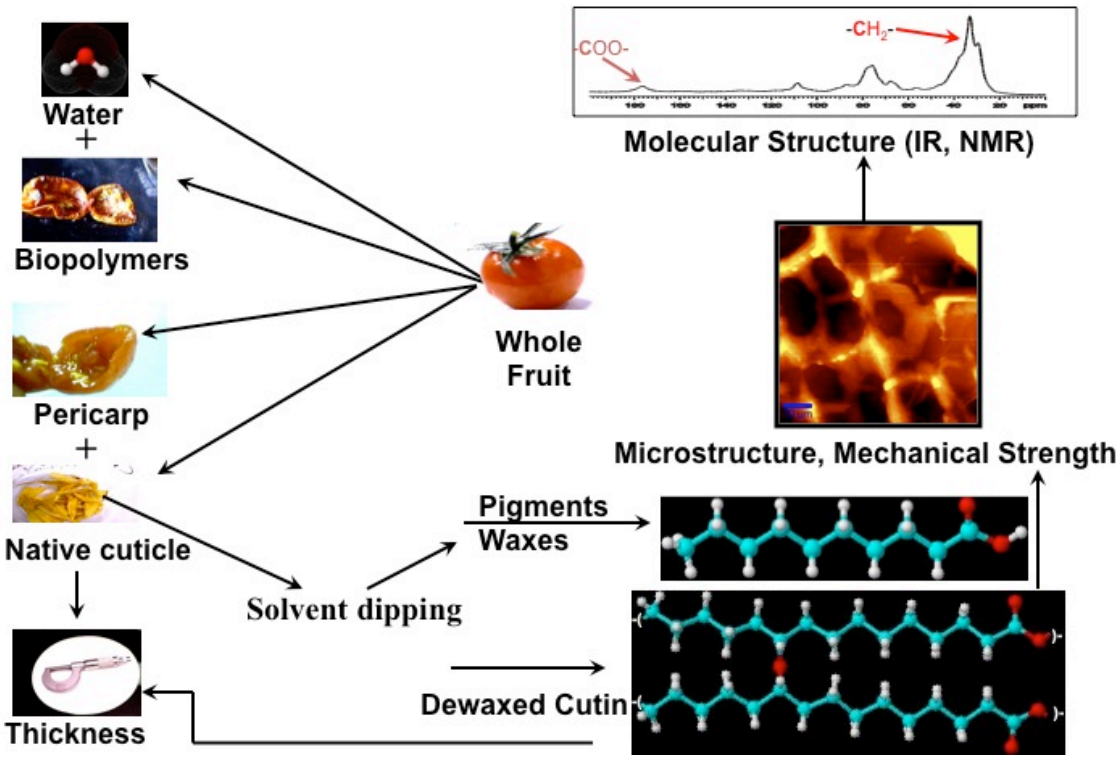

Figure 3.1. Overall scheme for experimental modules.
Adapted from Stark, 2007. R.E. Stark, proposal to the National Science Foundation.

Estimation of the water percent aims to compare the total relative amounts of liquid and solid components (biopolymeric materials) in the fruit. This experiment demonstrates the effect of water-loss on the overall morphology of the fruit, a significant factor in maintaining freshness and marketability of produce. Demonstration of partially dried tomato causing wrinkled morphology of the fruit can be used to motivate student discussions.

Following the measurement of mass percent of water, students focus on the cuticle, a protective external hydrophobic membrane of the tomato fruit. The cuticle acts as a strong defensive barrier to various biotic and abiotic stresses and regulates water-loss from the fruit. The cutin biopolyester and various waxes form cuticle's primary structural framework, which is supported by complex polysaccharides (cellulose and pectin) present in the cell wall. To remove cell walls

from the cuticle, tomato skins peeled from a fresh fruit are treated with an aqueous mixture of cellulase and pectinase enzymes to remove associated cellulose and pectin. After removal of cell walls, thickness of the native cuticle is measured.

Afterwards, the lycopene pigment extracted from enzymatically-treated cuticle is investigated by UV-Vis absorption spectroscopy and high performance liquid chromatography. For the next structural study, the enzymatically-isolated cuticle is subjected to dewaxing by solvent extraction and thickness of the dewaxed cuticle is measured. Structural fingerprints of the cutin biopolyester and waxes are established by solid-state and solution-state NMR, respectively. In a separate laboratory session, surface properties of the enzymatically isolated waxy cuticle and dewaxed cuticle (cutin) are examined by AFM[34]. A detailed format of the course module including description of experimental procedures is included in the Supplemental Materials.

3.5. Representative results

The suite has been tested as summer courses in "pilot-programs" for high school and undergraduate students at the City College of NY and the College of Staten Island.

Four groups of high school students measured water percent in tomatoes. Their acquired data (Table 3.2) showed that tomato fruit has substantially higher water content (above 90%) than biopolymers on a mass per mass basis. This is a notable observation and can be used as a motivation to research other common fruits and vegetables. The rate of water loss was also measured. It was observed that almost 80% water was lost in 4 hours for a piece of fruit whereas, only 60% of water was lost for whole fruit in same time (Figure 3.2). This is due to a greater proportion of the exposed surface area in the cut fruit. This observation can be extended into research mini-projects with an aim to compare rate of water loss between different fruits.

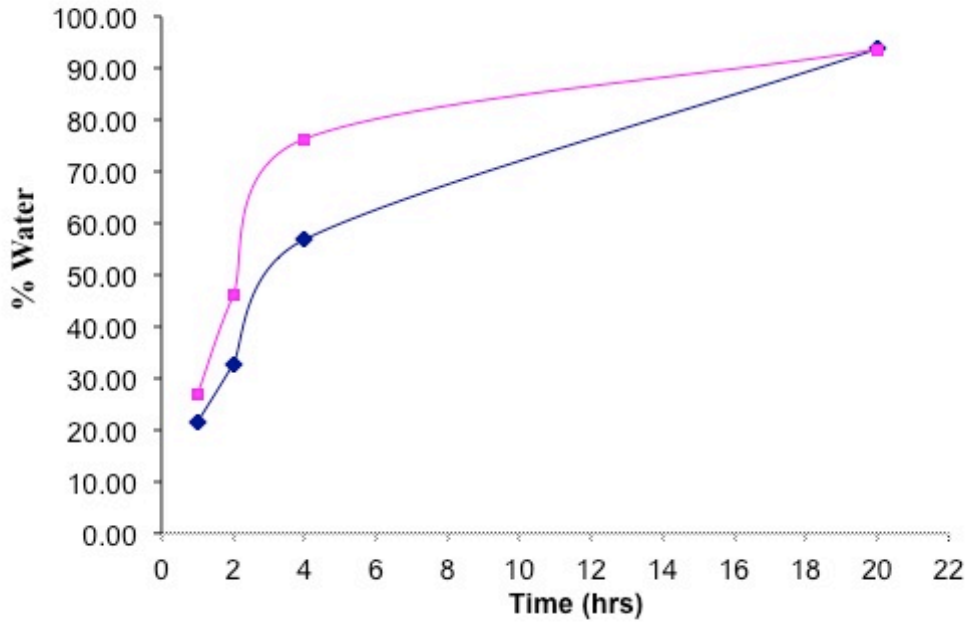

Figure 3.2 Rate of water loss in whole fruit (blue) versus a piece of fruit (purple).

In the next step, students used calipers to measure the thickness of the natural waxy and dewaxed cuticles, respectively. With a few exceptions, most of them noted that the waxy cuticle is thicker compared to the dewaxed sample (cutin), implying that wax is the constituent responsible for thickness of tomato cuticle (Figure 3.3).

Following water content and thickness of cuticle, the color of the tomato is an interesting feature to investigate. Lycopene pigment in tomato cuticle is responsible for the red color of the fruit[35]. Lycopene shows a characteristic absorption centered at 471 nm. Probing lycopene pigment by UV/Vis-absorption spectroscopy and comparing retention times of the extracted lycopene from tomato skins with commercial lycopene allowed students to comprehend operational principles of UV-Vis spectroscopy and HPLC (data shown in supplemental information).

In parallel with pigment characteristics, surface features of the cuticle can be explored using atomic force microscopy (AFM). Structural profile of cuticular waxes was investigated by

performing a ^{13}C-Hetronuclear Multiple Quantum Coherence (HMQC) NMR experiment on the extracted waxes dissolved in $CDCl_3$. This 2D solution-state NMR measurement delineates chemical shift correlation map between directly bonded ^{1}H and ^{13}C nuclei, thus helping to identify the functional groups more definitively.

After progressively removing the waxes from the tomato cuticle by solvent extraction, 1D ^{13}C cross-polarization magic-angle-spinning (CPMAS) solid-state NMR was carried out to identify the key functional groups in the cuticle. Adamantane was used as a standard for ^{13}C chemical shift referencing[36]. This 1D ^{13}C solid-state NMR measurement reveals the structural fingerprint of heterogeneous and insoluble cutin biopolyester in its natural physical state.

In absence of solid-state NMR, similar information can be obtained by FT-IR. Alternatively, mixture of solvents of varying polarity can be used to extract polar and non-polar components of waxes to be analyzed by solution NMR.

Hazards: Chloroform, used in lycopene characterization, is highly flammable and a potential carcinogen. Care should be taken to avoid inhalation and exposure to skin. Lycopene should be kept in a dark container and protected from light, since it is readily oxidized owing to multiple double bonds. Gloves and goggles should be used while handling toxic sodium azide.

3.6. Discussion

The presented laboratory module allows students to take a “tour” into the tomato fruit. Starting with basic measurements of mass percent of water, thickness of cuticle, the suite delves into surface characteristics of the fruit cuticle complemented by probing ensemble-averaged microscopic structural properties of the extracted biopolymers by NMR.

The flexibility of the modules and broad interdisciplinary learning objectives cannot be emphasized too strongly. In terms of flexibility, the modules are adaptable for students at

different academic levels along with incorporation of "research-oriented" mini projects studying common fruit/vegetables. Interdisciplinary approach of the design is apparent in several of the presented experimental module. Studying structural characteristics of vegetable and fruits could be interesting to students interested in nutrition, food processing chemistry as well as chemical engineering. Comparison of surface properties of protective tomato cuticle and commercially available protective films might interest students of industrial chemistry.

In a nutshell, the presented design offers a novel approach in teaching several cross-disciplinary techniques involving a common subject tomato with interwoven adaptable features to motivate students at different levels.

3.7. Instructor's note for touring the tomato: Suite of Chemistry Laboratory experiments

3.7.1. Layout of modular approach

The instructor may want to implement the experiments according to discipline-specific learning objectives. The experimental schedule (Table 3.1) can be adjusted by mixing demonstrations and student exercises to emphasize general chemistry (G), biochemistry (BC), organic chemistry (O), biophysical chemistry (BP), or analytical chemistry (A). Modules 1-5 are suitable for students at all levels. On one hand these modules can be offered as research experience to high school students, on the other hand these modules can build the foundation for undergraduate students.

Following modules 1-5 as the core curriculum, modules 6-8 can be implemented based on availability of specified instruments at the institutional level. For implementation at high school, community college or Liberal Arts College, dewaxed cuticle can be investigated in solid state using Fourier transform infrared spectroscopy (FTIR) as an alternative to solid state NMR. FTIR provides similar information about signature functional groups as obtained by solid state NMR. Typically, for tomato cutin, the bands of interest from FTIR would be located at 1734 to 2926

cm^{-1} (or 2855 cm^{-1}) and at 1061 and 1035 cm^{-1} for ν (C=O) stretching vibrations of ester groups, ν (CH) stretching vibrations of $(CH_2)_n$ groups in fatty acid monomers of the cutin polymer and ν (C-O) stretching vibrations of alcohol group respectively, in cutin [37]. The modules can be offered in continuous sessions or can be organized according to the instructor's discretion depending on the learning objectives of the specific curriculum.

3.7.2. Experimental notes

3.7.2.1. Mass percent of water in tomato

Typical values for mass percent of water ranges from 80-90% (Table 3.2). Some additional experimental notes are listed below.

Group ID	Mass of fruit (g)	Mass of watch glass (g)	Final mass of fruit and watch glass (g)	Mass of dehydrated fruit (g)	Percentage of water (%)
SK	14.12	47.45	46.2	1.25	91.15
DOL	15.95	43.51	42.19	1.32	91.72
HJ	9.94	47.29	46.49	0.8	91.95
Jaguars	15.51	48.65	46.92	1.73	88.85

Table 3.2. Experimental data for mass percent of water in tomato.

1. Students should be watchful while recording mass using a top loading balance.

2. The balance should be placed to avoid air drifts, which can potentially affect measurements.

3. While drying the tomato in the oven, care should be taken to avoid possible burns and the drying process should be closely monitored to avoid possible charring of the fruit.

4. For assistance with Microsoft office Excel software the instructor's guidance should be requested, as needed.

5. While measuring mass at different stages of the experiment, students should repeat measurements in order to avoid manual error.

6. Comparison of mass percent of water between similar tomatoes from different sources and different tomato varieties can make a good post-lab activity.

3.7.2.2. Thickness of tomato cuticle

Students should obtain multiple measurements from the same sample in order to estimate experimental error. With few exceptions, the representative data exhibited (Figure 3.3) that waxy cuticle is thicker compared to the dewaxed sample (cutin). This implies that wax is responsible for the thickness of tomato cuticle.

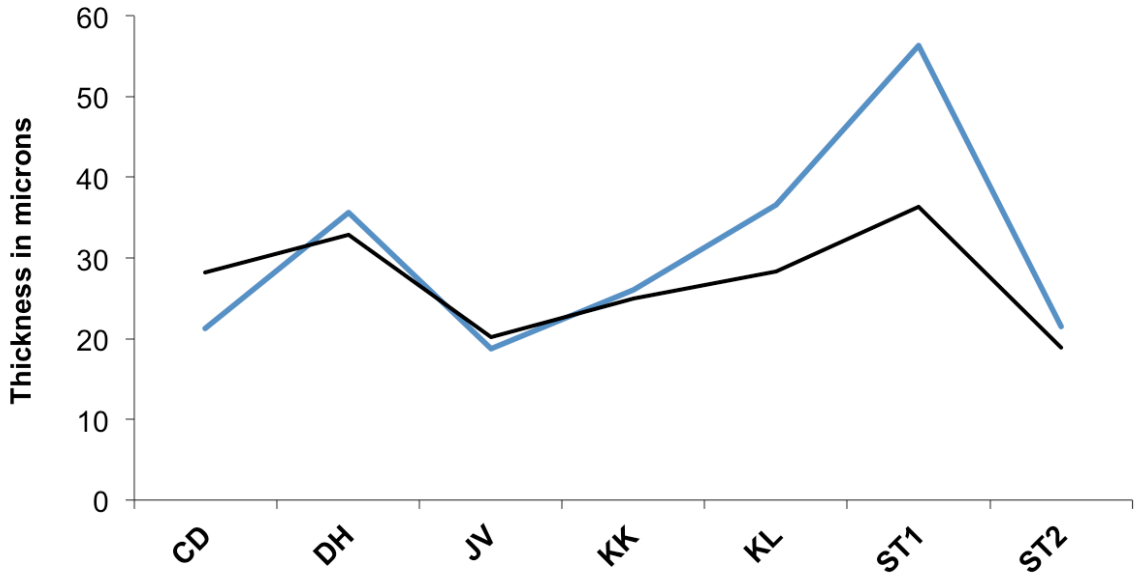

Figure 3.3. Thickness of un-dewaxed (blue) and dewaxed cuticle (black).

3.7.2.3. Lycopene characterization

Representative absorption spectrum of extracted lycopene shown in Figure 3.4 illustrates characteristic absorption centered at 471 nm, which is in accord with data from commercial

lycopene. Additionally, HPLC profile of extracted and commercial lycopene showed comparable retention times.

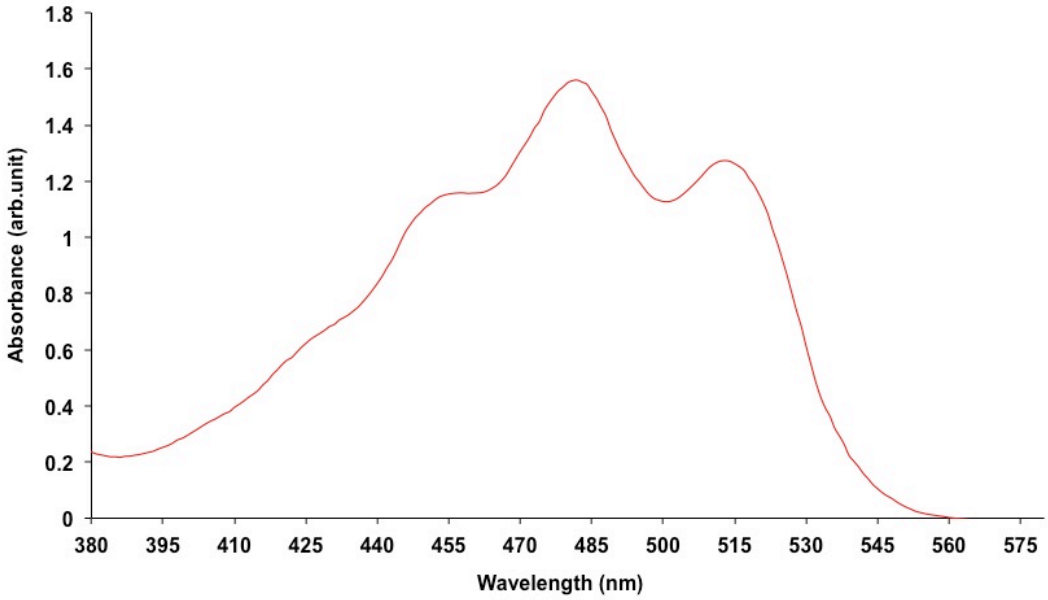

Figure 3.4. UV-Vis absorption spectrum of lycopene extracted from tomato cuticle.

Typical retention times are 5.024 minutes for extracted lycopene and 5.016 minutes for commercial lycopene obtained from HPLC (Figure 3.5). Students should be instructed to be careful to prevent the container from exposure to light by wrapping with aluminum foil. Chloroform is inflammable and carcinogenic; therefore gloves and goggles should be used to handle the chloroform solvent.

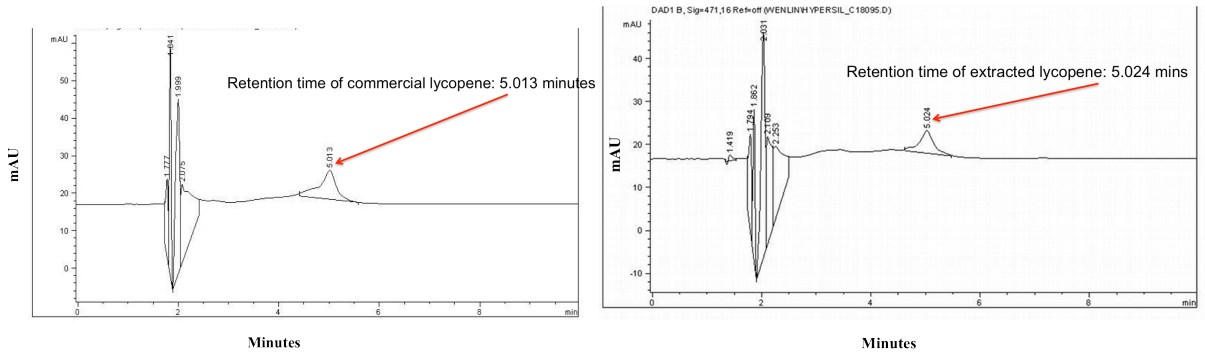

Figure 3.5. HPLC profile of extracted lycopene & commercial lycopene.

3.7.2.4. Enzymatic treatment and dewaxing of tomato cuticle by solvent extraction

The inflammable organic solvents should be used cautiously wearing gloves and goggles. Care should be taken while handling the enzyme cocktail since it contains toxic bactericidal agent sodium azide. Alternatively, fresh enzyme cocktail can be used to avoid using sodium azide. Typically, the speed of rotation during incubation is 200 rpm, which will vary among different incubators. At the end of enzymatic treatment, care should be taken while washing the tomato skins to avoid breakage; since intact pieces are required for AFM measurements.

3.7.2.5. Surface analysis of tomato cuticle by contact mode AFM[38]

Investigation of surface properties of tomato cuticle by AFM revealed nanoscale surface features in waxy and dewaxed cuticles. The average surface roughness was estimated to highlight changes in the cuticular membrane upon exhaustive dewaxing (Figure 3.6). Typical roughness values are in the range of 10 nm to 20 nm, with roughness increasing due to dewaxing.

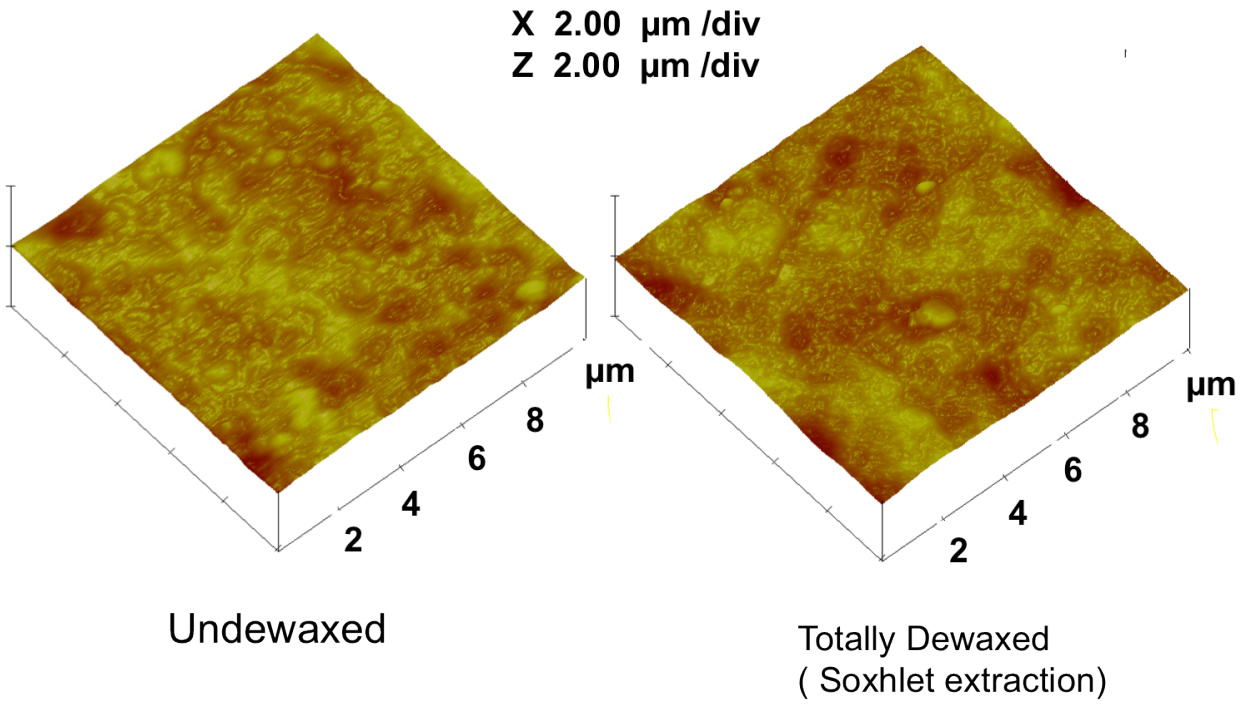

Figure 3.6. AFM images of undewaxed and exhaustively dewaxed commercial tomato cuticle.

3.7.2.6. Solid state NMR of cutin

Solid-state NMR of cutin by CPMAS experiment is illustrated for a Varian NMRS spectrometer operating at a ^{1}H frequency of 600 MHz. The CPMAS experiment identifies major functional groups in cutin biopolyester (Figure 3.7). The key carbon moieties in the cutin biopolyester are long-chain alkyl (0-45 ppm), oxygenated alkyl (45-110 ppm), aryl and alkene (110-160 ppm), and carbonyl (160-220 ppm).

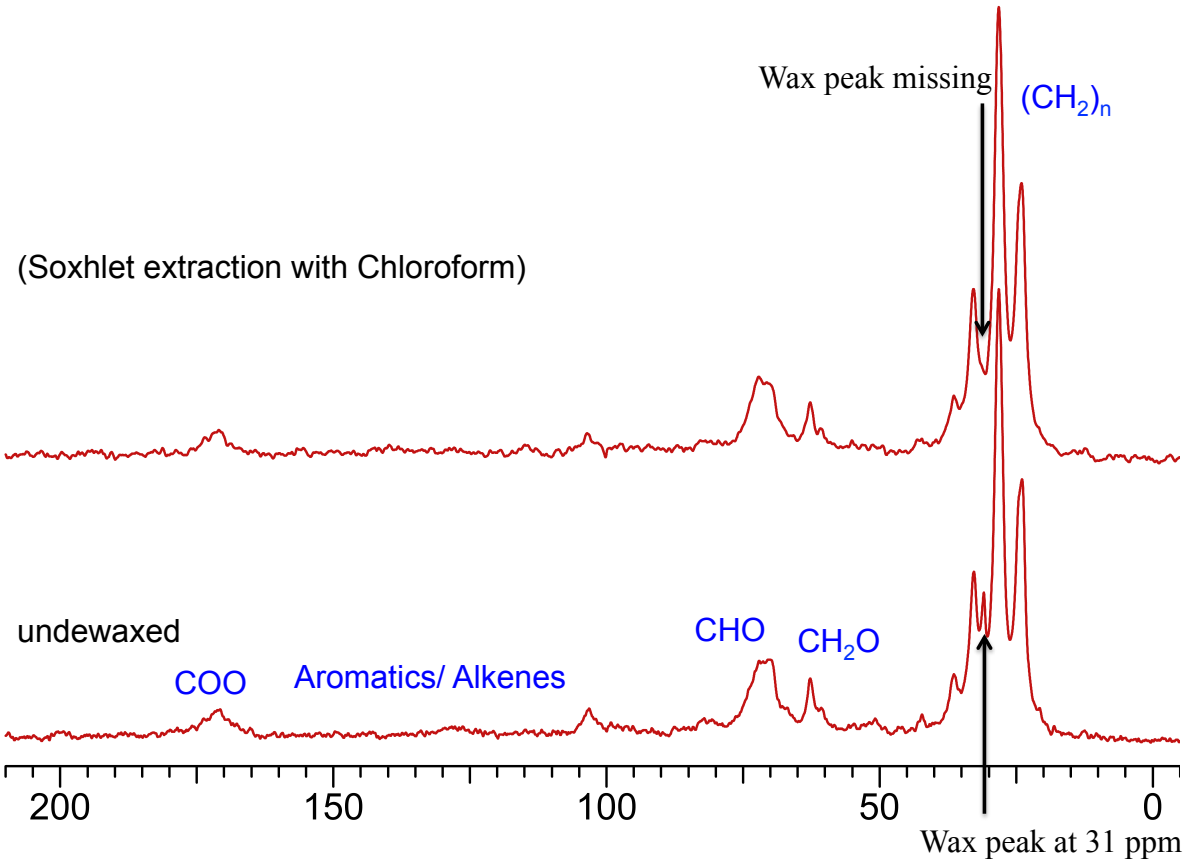

Figure 3.7. Structural fingerprint of undewaxed and solvent extracted tomato cuticle monitored by solid-state CPMAS experiment.

The CPMAS experiments should be repeated with un-dewaxed, enzymatically treated tomato cuticle in order to compare the structural fingerprints of un-dewaxed cuticle with dewaxed cutin sample. The main difference between the CPMAS spectra of un-dewaxed and dewaxed cuticle would be the presence of wax peaks at 31-33 ppm in the un-dewaxed form (Figure 3.7).

3.7.3. Equipment, supplies and reagents

Top-loading balance, pH meter, incubator/shaker, beaker (250 mL), glass bottle with cap (200 mL), measuring cylinder (5 mL and 100 mL), kitchen strainer, vacuum drier, oven, large bowl, glass dropper, magnetic stirrer, cherry or grape tomatoes, deionized water, sodium acetate trihydrate, hydrochloric acid (3M), pectinase (EC 3.2.1.15; 10 U ml^{-1}, store in refrigerator),

cellulase (EC232.734.4; 1.3 units/mg, store in refrigerator), glacial acetic acid (Sigma-Aldrich #A9967), sodium azide (Sigma-Aldrich #S2002-100G), methanol ACS grade (VWR #EMD-MX0485-7), chloroform (ACS grade, VWR), chloroform HPLC grade (Sigma-Aldrich), acetonitrile, methanol HPLC grade (Sigma-Aldrich), hexane (VWR), HPLC instrument (Agilent 1100 series), lycopene (Sigma #L9879), syringe, Hypersil (Reverse-phase C_{18}) column (Thermo scientific), nitrogen gas, glycine (Sigma-Aldrich #50046), glutamine (Sigma-Aldrich #49419), adamantane (Sigma-Aldrich #100277), Erlenmeyer flask, glass bottle, 0.22 μm nylon membrane, filter paper and filtering flask, graduated cylinders (25 mL and 250 mL), aluminum foil (Fisher), Variac controller, Disposable thimble (80 mm/ 25 mm) (VWR), glass wool (VWR), tweezers (VWR), NMR spectrometer (standard bore magnet), MAS rotor, multimode scanning probe microscope, light microscope, nanoscope software, AFM probe, magnetic puck, double sided tape, Buchner funnel.

3.7.4. Student handout

3.7.4.1. Mass percent of water

1. Obtain a cherry tomato for each group of students. Use Kim wipes to remove any dirt from the fruit's surface and place the tomato on a piece of clean paper towel. Next, label a clean watch glass with the group name, experiment number, and date of the experiment.

2. Using a top-loading balance, measure the mass of the watch glass to the closest 0.1g (M_g) and record in the laboratory notebook.

3. Cut the tomato into two halves and place both pieces on the watch glass. Now, determine the mass of the tomato (with the watch glass) using the same balance; note this combined weight of tomato and watch glass (M_1) and the mass of the native tomato (M_1-M_g), in the lab notebook.

4. Then, place the tomato (on the watch glass) inside an oven (at 95°C) for 1 hour. Take the tomato out of the oven carefully and place it in a desiccator to cool. When it reaches room temperature, record the mass of the tomato and watch glass (M_2). Note the difference in values (M_2-M_1). Also, record the difference (M_2 -M_g) as M_d (the mass of dehydrated tomato).

5. Repeat the steps of drying in oven, cooling in desiccator and recording of M_2 until it reaches a constant value. Using the recorded data, then instruct the students to calculate percent by mass of water for the tomato sample and plot the results using Microsoft office Excel software. The formula for calculating mass percent of water is: $[(M_1-M_g)-(M_2-M_g)]/[(M_1-M_g)]*100$.

6. Optionally, compare rate of water loss between whole fruit and a half piece by keeping them in oven for same period of time.

Sample pre-lab and post-lab questions are given below.

Pre-lab questions:

1. Please go through the procedure of your experiment carefully. How do you know the fruit is completely dried?

2. One chocolate chip cookie has 66.67 % carbohydrates. How much (in grams) carbohydrate do you consume in one serving, which contains 3 cookies (total weight =33 g)?

3. Each serving size of cookies has 8 gm total fat. If each cookie has equal weight, compare the amount of fat and carbohydrate present in one cookie. [All data for questions 2 and 3 are taken from the nutrition facts of Chip Ahoy Cookies]

Post lab questions:

1. Do you think cutting a tomato into pieces will have any effect on its drying process? Explain, considering the amount of water lost, rate of dehydration, and any other factors.

2. Compare mass percent of water between tomatoes procured from different sources and make a plot using Microsoft excel or similar software.

3. What would be a good way (i.e. pie diagram, bar diagram, x-y plot) to present and compare the experimental data from your whole class using the Excel program?

4. Which part of the fruit protects it from dehydration?

5. How do you think the percentage of water varies for different fruits and vegetables?

6. Although you drink very clean water everyday, does this experiment make you think that water pollution could adversely affect your health by some other way?

3.7.4.2. Enzymatic removal of cell wall from tomato cuticles

1. Procedures are illustrated for a class of 6 students, with each group of 2 receiving a cherry tomato. Before the class, prepare 50 mM pH 4.0 sodium acetate buffer and 200 ml enzyme cocktail. To prepare the buffer, mix 1.22 g of sodium acetate trihydrate (M_r 136.08 g/mol) and 2.34 ml glacial acetic acid (17.485 M) in a beaker, add 200 ml of deionized water and then adjust the pH to 4.0 at 31ºC. For 200 ml of enzyme cocktail, mix 4 ml of pectinase (EC 3.2.1.15; 10 U ml^{-1}, TCI America), 0.2 g of cellulase (EC 232.734.4; 1.3 units/mg solid, Sigma Aldrich #C1184-100KU), 13 mg NaN_3, and finally make up the volume to 200 ml with sodium acetate buffer[38].

2. Obtain a cherry tomato for each student group. Immerse the tomato under deionized water in a beaker.

3. Peel off the skin from the fruit in large sections and discard the inner pericarp tissue. Next, wash the tomato skins a few times with deionized water and preserve the skins under water in a beaker.

4. Obtain 40 ml of enzyme cocktail for each student group.

5. Immerse the peeled tomato skins completely in the enzyme cocktail in a capped bottle labeled with students' name, experiment names and dates of experiment. Incubate at 31°C for 24 hours with continuous shaking (G24 Environmental Incubator Shaker, New Brunswick Scientific Co.).

6. Return at the following session to collect the skins after enzymatic treatment. Use Buchner funnel (alternatively use vacuum filtering) to collect the skins. Wash the skins with deionized water and dry the skins by placing in a vacuum oven for an hour at room temperature.

7. Preserve the dried tomato skins in labeled and capped bottles for the next experiment

Sample pre-lab and post-lab questions are listed below.

Pre-lab questions:

1. Please read the procedure of our experiment carefully. What is the final concentration of the pectinase solution when 2 mL of pectinase (3364 units/mL) is diluted to obtain 200 mL of the final solution? Report the concentration of enzyme in units/100mL.

2. What is the concentration of sodium acetate (in molarity units) when 1.3608 gram of sodium acetate is dissolved in 200 mL of distilled water? (Formula weight of sodium acetate tri-hydrate = 136.08 g.)

3. Why do you think addition of hydrochloric acid is required to adjust the pH of the sodium acetate buffer solution? Can you use any other acid to have a similar effect on the buffer solution?

Post-lab questions:

1. Why is it important to maintain the pH of the pectinase solution around 4?

2. How does vacuum drying help the water removal process from tomato skins?

3. Have you noticed any physical change in the tomato skins after digesting them with enzyme? Describe your observations.

3.7.4.3. Thickness of tomato cuticle

Cuticular wax is responsible for the thickness of the tomato cuticle. Steps of measuring thickness are detailed below.

1. Place 1 g of natural (freshly peeled) tomato cuticle on a piece of paper towel.

2. Measure the thickness of the cuticle using a caliper; repeat the measurement in different locations of the cuticle (along length & width).

3. It is important to obtain multiple measurements from the same sample to estimate experimental error.

4. Repeat the procedure with exhaustively dewaxed cuticle.

5. Record the data in a laboratory notebook.

6. Collect the data for waxy and dewaxed cuticle from all students groups and make a plot (as shown in Figure 3.3) using Microsoft office Excel or similar software.

Sample questions are given below.

1. Do you think thickness measurements will differ between tomato varieties, for example, cherry tomato versus plum tomato/beefsteak tomato?

2. What is main contributing factor behind thickness of tomato cuticle?

3.7.4.4. Lycopene characterization

1. Put 100 mg of pectinase-treated tomato skins (with cell walls removed from the cuticle) in a glass bottle. (Alternatively, use freshly peeled tomato skins).

2. Measure 20 ml of chloroform using a graduated cylinder. Immerse the tomato skins in this chloroform in the bottle. Extract the pigment with continuous stirring for 30 minutes. During this extraction process, cover the bottle with aluminum foil to avoid direct exposure to light. Notice the color change of the organic medium.

3. Filter the organic solution with a 0.22 μm nylon filter membrane to remove particulates.

4. Perform wavelengths scan of the solution from 380 nm to 700 nm and observe a peak at 471 nm, characteristic of lycopene.

5. Using the automated system in the HPLC unit, degas the 1:1 acetonitrile: methanol solution, before using it to condition the column.

6. Wash a reverse phase (RP)-HPLC column (Hypersil Gold, C_{18}, Thermo Scientific) with a mixture of acetonitrile and methanol (1:1) at a constant flow rate of 1ml/min for 15 minute.

7. Prepare 1 liter of an isocratic mobile phase of methyl alcohol and acetonitrile in a volume ratio of 3:1 (alternatively, pure methanol could be used) and degas this solution using the automated system in the HPLC unit.

8. Equilibrate the column with the mobile phase at the same flow rate of 1 ml/min for 20 minutes.

9. Inject 10 μl of the pigment solution into the column, detecting it at a wavelength of 471 nm and ambient temperature. In case, the HPLC unit does allow wavelength adjustment, perform a wavelength scan from 380 nm to 700 nm. Repeat the steps of column equilibration and injection of pigment solution twice.

10. Compare the retention times of the extracted pigment with a standard 0.018 mM lycopene (Sigma #L9879) solution [comparable to the concentration of extracted lycopene] under the same experimental conditions.

Sample post-lab questions are given below.

1. What is the biological importance of lycopene?

2. Can you think of any other common colored fruit(s)/vegetable(s)? What are the pigments responsible for such coloration? Plan experiments to study another pigment from a common fruit/vegetable.

3.7.4.5. Dewaxing of tomato cuticle by solvent extraction

1. Put 0.5-1 g of dried tomato skin obtained from enzymatic treatment of the cuticles (as described earlier) into 1:1 (v/v) chloroform-water containing vials and mix for four minutes.

2. Following vigorous agitation and phase separation, transfer chloroform fractions by pipetting and evaporate them in separate uncovered, labeled vials. Complete evaporation leaves epicuticular wax in these vials.

3. Now, put the tomato cuticles (with epicuticular wax removed) in chloroform and shake for 2 hours and collect intracuticular wax after evaporating the solvent chloroform.

4. Using solvents of varying polarity, for example methanol, benzene may be useful as student exercise.

5. Afterwards, dry the dewaxed tomato cuticle sample. For drying, use a stream of nitrogen gas or place the sample in vacuum oven for an hour.

6. After drying the cutin sample, measure the mass of the dried sample and store it at room temperature in a screw-top jar sealed with parafilm, labeled with student name, name and date of the experiment.

Sample post-lab question is presented below

1. Do you notice any differences between treatments of the cuticle with solvents of varying polarity; for example, chloroform, methanol and hexane? Provide reasoning for such differences.

3.7.4.6. Analysis of surface roughness by AFM[38]

1. To investigate the surface roughness of un-dewaxed and dewaxed cuticle use the contact Atomic Force Microscopy (AFM) mode. Replace the existing AFM cantilever with a new silicon nitride cantilever and use a light microscope to ascertain that the newly placed cantilever is not broken.

2. Fix the tomato cuticle sample (a section of solvent dipped tomato cuticle ~25 mm x 25 mm) on a sample puck with double-sided tape. Use a light microscope to verify that the cuticle surface is flat and smooth. Afterwards, place the puck with the tomato cuticle sample onto the AFM scanner.

3. Place the tipholder with the new AFM probe into the AFM head and align the laser spot on the AFM cantilever. Carefully monitor the reflected laser beam so that the incident laser spot exactly stays at the end of the AFM cantilever. Ensure that the reflected laser beam is being received evenly by the four quadrants of the photodetector and a maximum total signal (SUM signal) is achieved.

4. Allow the AFM tip to approach the sample, but not so close that the tip touches or breaks through the sample surface. At this point, the laser light reflected off the AFM cantilever will bounce off the movable mirror to the photodetector. For the contact AFM mode with a silicon nitride AFM tip, set the OUTPUT signal (Vertical Deflection) voltage to -2V for a 0V Setpoint

and the DIFF Signal (vertical/horizontal difference) to 0 V by adjusting the position of the mirror.

5. After fixing the scan size at 10 micron and scan rate at 2Hz, engage the AFM tip onto the sample surface. Note that, upon engaging the tip successfully scanning will start automatically. Using both image and scope modes of the software, monitor the scanning process and adjust relevant parameters, for example, setpoint, integral gain, proportional gain, scan size, scan rate. To achieve highest resolution images and to observe best contrast of the surface of the image, adjust the line and samples/line iteratively.

6. Capture the image; save the data file and process the data using appropriate parameters and finally calculate the average roughness. Typical RMS roughness values are in the range of 10 nm to 20 nm with roughness increasing due to dewaxing.

7. Repeat the procedure after changing scanning area of the cuticle surface and take measurement at five sample locations to check reproducibility. Make sure to replace the AFM cantilever if you note deterioration in image quality.

8. Repeat the same procedure with un-dewaxed, enzymatically treated cuticle.

3.7.4.7. Solution state NMR of cuticular wax

1. Obtain cuticular wax, isolated by solvent extraction, in $CDCl_3$.

2. Record two-dimensional ^{13}C-Heteronuclear Multiple Quantum Coherence experiment with 1024 complex points in t_1 and 128 complex points in t_2 with 128 transients. This experiment enables identification of major functional groups in the cuticular wax.

3. As an alternative to the two dimensional experiment, one dimensional ^{1}H spectrum can be recorded to identify classes of functional groups.

Sample post-lab question is presented below.

1. What are the major functional groups in cuticular wax? Identify the functional groups in the acquired NMR spectrum.

3.7.4.8. Solid state NMR of cutin

1. Pack 4-6 mg of dewaxed tomato fruit cuticle (cutin) uniformly into a Magic Angle Spinning (MAS) rotor using the vendor supplied packing tool.

2. Adjust the homogeneity of the magnetic field to minimize spectral line width at half-height.

3. Tune and match the probe iteratively to ensure minimum power reflection at both ^{1}H and ^{13}C NMR frequencies. Calibrate the ^{1}H and ^{13}C 90° pulse widths using adamantane (Sigma-Aldrich #100277) as the standard compound.

4. To obtain maximum signal intensity, use glycine or glutamine and optimize all experimental parameters (Hartmann-Hahn matching power levels, ^{1}H-^{13}C contact time, heteronuclear ^{1}H decoupling strength) for the cross-polarization magic angle spinning (CPAMS) experiment.

5. Fix the experimental temperature to 25°C (or room temperature).

6. Using a 10 kHz spinning frequency with 3-sec delay between transients, and SPINAL heteronuclear proton decoupling at a magnetic field strength equivalent to a frequency of 185 kHz is recommended to record the spectrum at a ^{1}H frequency of 600 MHz.

7. After inserting the cutin-packed rotor into the probe, slowly increase the spinning speed up to 10 kHz to verify efficient sample packing and rotor stability. Validate the final spinning stability of the rotor within ±20 Hz and record the pre-optimized CPMAS experiment, with 4096 transients.

8. Adjust the spectrum with exponential (Lorentzian) line broadening of 50-100 Hz, and perform a Fourier transform to generate an NMR spectrum of signal intensity vs. chemical shielding (ppm).

9. Externally use adamantane as a standard, setting $-CH_2-$ group to 38.4 ppm for ^{13}C chemical shift referencing.

Bibliography

1 Ockner, R. K., Manning, J. A. & Kane, J. P. Fatty acid binding protein. Isolation from rat liver, characterization, and immunochemical quantification. *J Biol Chem* **257**, 7872-7878 (1982).

2 Storch, J. & Corsico, B. The emerging functions and mechanisms of mammalian fatty acid-binding proteins. *Annu Rev Nutr* **28**, 73-95 (2008).

3 Storch, J. & McDermott, L. Structural and functional analysis of fatty acid-binding proteins. *J Lipid Res* **50 Suppl**, S126-131 (2009).

4 Storch, J. & Thumser, A. E. Tissue-specific functions in the fatty acid-binding protein family. *J Biol Chem* **285**, 32679-32683 (2010).

5 Storch, J. & Thumser, A. E. The fatty acid transport function of fatty acid-binding proteins. *Biochim Biophys Acta* **1486**, 28-44 (2000).

6 Wolfrum, C., Borrmann, C. M., Borchers, T. & Spener, F. Fatty acids and hypolipidemic drugs regulate peroxisome proliferator-activated receptors alpha - and gamma-mediated gene expression via liver fatty acid binding protein: a signaling path to the nucleus. *Proc Natl Acad Sci USA* **98**, 2323-2328 (2001).

7 Thompson, J., Winter, N., Terwey, D., Bratt, J. & Banaszak, L. The crystal structure of the liver fatty acid-binding protein. A complex with two bound oleates. *J Biol Chem* **272**, 7140-7150 (1997).

8 He, Y., Yang, X., Wang, H., Estephan, R., Francis, F., Kodukula, S., Storch, J. & Stark, R. E. Solution-state molecular structure of apo and oleate-liganded liver fatty acid-binding protein. *Biochemistry* **46**, 12543-12556 (2007).

9 Marcelino, A. M., Smock, R. G. & Gierasch, L. M. Evolutionary coupling of structural and functional sequence information in the intracellular lipid-binding protein family. *Proteins* **63**, 373-384 (2006).

10 Hodsdon, M. E. & Cistola, D. P. Ligand binding alters the backbone mobility of intestinal fatty acid-binding protein as monitored by 15N NMR relaxation and 1H exchange. *Biochemistry* **36**, 2278-2290 (1997).

11 Zimmerman, A. & Veerkamp, J. New insights into the structure and function of fatty acid-binding proteins. *Cellular and molecular life sciences* **59**, 1096-1116 (2002).

12 He, Y., Estephan, R., Yang, X., Vela, A., Wang, H., Bernard, C. & Stark, R. E. A Nuclear Magnetic Resonance-Based Structural Rationale for Contrasting Stoichiometry and Ligand Binding Site(s) in Fatty Acid-Binding Proteins. *Biochemistry* **50**, 1283-1295 (2011).

13 Storch, J. & Bass, N. M. Transfer of fluorescent fatty acids from liver and heart fatty acid-binding proteins to model membranes. *J Biol Chem* **265**, 7827-7831 (1990).

14 Kim, H. K. & Storch, J. Mechanism of free fatty acid transfer from rat heart fatty acid-binding protein to phospholipid membranes. Evidence for a collisional process. *J Biol Chem* **267**, 20051 (1992).

15 Richieri, G. V., Ogata, R. T. & Kleinfeld, A. M. Equilibrium constants for the binding of fatty acids with fatty acid-binding proteins from adipocyte, intestine, heart, and liver measured with the fluorescent probe ADIFAB. *J Biol Chem* **269**, 23918 (1994).
16 Wolfrum, C., Ellinghaus, P., Fobker, M., Seedorf, U., Assmann, G., Börchers, T. & Spener, F. Phytanic acid is ligand and transcriptional activator of murine liver fatty acid binding protein. *J Lipid Res* **40**, 708 (1999).
17 Hostetler, H. A., Balanarasimha, M., Huang, H., Kelzer, M. S., Kaliappan, A., Kier, A. B. & Schroeder, F. Glucose regulates fatty acid binding protein interaction with lipids and peroxisome proliferator-activated receptor alpha. *J Lipid Res* **51**, 3103-3116 (2010).
18 Myszka, D. G. & Swenson, R. P. Identification by photoaffinity labeling of fatty acid-binding protein as a potential warfarin receptor in rat liver. *J Biol Chem* **266**, 20725-20731 (1991).
19 Cavanagh, J. *Protein NMR spectroscopy: Principles and practice*. (Academic Pr, 2007).
20 Velkov, T., Chuang, S., Prankerd, R., Sakellaris, H., Porter, C. J. H. & Scanlon, M. J. An improved method for the purification of rat liver-type fatty acid binding protein from Escherichia coli. *Protein expression and purification* **44**, 23-31 (2005).
21 Hsu, K. T. & Storch, J. Fatty acid transfer from liver and intestinal fatty acid-binding proteins to membranes occurs by different mechanisms. *J Biol Chem* **271**, 13317-13323 (1996).
22 Delaglio, F., Grzesiek, S., Vuister, G. W., Zhu, G., Pfeifer, J. & Bax, A. NMRPipe: a multidimensional spectral processing system based on UNIX pipes. *J Biomol NMR* **6**, 277-293 (1995).
23 Johnson, B. A. & Blevins, R. A. NMR View - A Computer program for the visualization and analysis of NMR data. *J Biomol NMR* **4**, 603-614 (1994).
24 Mulder, F. A. A., Schipper, D., Bott, R. & Boelens, R. Altered flexibility in the substrate-binding site of related native and engineered high-alkaline Bacillus subtilisins. *J Mol Biol* **292**, 111-123 (1999).
25 DeLano, W. L. The PyMOL molecular graphics system. (2002).
26 Mathews, C., Van Holde, K. & Ahern, K. *Biochemistry. 3rd*. (San Francisco, Addison Wesley Longman, Inc, 2000).
27 Hanhoff, T., Lücke, C. & Spener, F. Insights into binding of fatty acids by fatty acid binding proteins. *Mol Cell Biochem* **239**, 45-54 (2002).
28 Hodsdon, M. E., Ponder, J. W. & Cistola, D. P. The NMR solution structure of intestinal fatty acid-binding protein complexed with palmitate: application of a novel distance geometry algorithm. *J Mol Biol* **264**, 585-602 (1996).
29 Eads, J., Sacchettini, J. C., Kromminga, A. & Gordon, J. I. Escherichia coli-derived rat intestinal fatty acid binding protein with bound myristate at 1.5 A resolution and I-FABPArg106-->Gln with bound oleate at 1.74 A resolution. *J Biol Chem* **268**, 26375-26385 (1993).
30 Nemetz, T. M., Ball, D. W., Whalen, D. & Blackman, D. Bleaching with Chlorine - Another Tomato Juice Demonstration. *J Chem Educ* **70**, 154-155 (1993).
31 Macbeath, M. E. & Richardson, A. L. Tomato Juice Rainbow - a Colorful and Instructive Demonstration. *J Chem Educ* **63**, 1092-1094 (1986).
32 Wang, Y., Zhang, M. & Hu, Y. Foam Fractionation of Lycopene: An Undergraduate Chemistry Experiment. *J Chem Educ* **87**, 510-511 (2010).

33 Isaacson, T., Kosma, D. K., Matas, A. J., Buda, G. J., He, Y. H., Yu, B. W., Pravitasari, A., Batteas, J. D., Stark, R. E., Jenks, M. A. & Rose, J. K. C. Cutin deficiency in the tomato fruit cuticle consistently affects resistance to microbial infection and biomechanical properties, but not transpirational water loss. *Plant J* **60**, 363-377 (2009).

34 Round, A. N., Yan, B., Dang, S., Estephan, R., Stark, R. E. & Batteas, J. D. The Influence of Water on the Nanomechanical Behavior of the Plant Biopolyester Cutin as Studied by AFM and Solid-State NMR. *Biophys J* **79**, 2761-2767 (2000).

35 Shi, J. & Le Maguer, M. Lycopene in tomatoes: Chemical and physical properties affected by food processing. *Crit Rev Biotechnol* **20**, 293-334 (2000).

36 Morcombe, C. R. & Zilm, K. W. Chemical shift referencing in MAS solid state NMR. *J Magn Reson* **162**, 479-486 (2003).

37 Matas, A. J., Yeats, T. H., Buda, G. J., Zheng, Y., Chatterjee, S., Tohge, T., Ponnala, L., Adato, A., Aharoni, A., Stark, R., Fernie, A. R., Fei, Z., Giovannoni, J. J. & Rose, J. K. Tissue- and cell-type specific transcriptome profiling of expanding tomato fruit provides insights into metabolic and regulatory specialization and cuticle formation. *The Plant cell* **23**, 3893-3910 (2011).

38 Chatterjee, S., Sarkar, S., Oktawiec, J., Mao, Z. & Stark, R. E. Protocols for isolation and biophysical study of fruit cuticles. *J Vis Exp* (In Press).